A stochastic hierarchical model for low grade glioma evolution

Journal of Mathematical Biology (2023) 86:89
https://doi.org/10.1007/s00285-023-01909-5

Mathematical Biology

A stochastic hierarchical model for low grade glioma evolution

Evelyn Buckwar[1,2] · Martina Conte[3] · Amira Meddah[1]

Received: 22 June 2022 / Revised: 17 March 2023 / Accepted: 22 March 2023 /
Published online: 5 May 2023

Abstract
A stochastic hierarchical model for the evolution of low grade gliomas is proposed. Starting with the description of cell motion using a piecewise diffusion Markov process (PDifMP) at the cellular level, we derive an equation for the density of the transition probability of this Markov process based on the generalised Fokker–Planck equation. Then, a macroscopic model is derived via parabolic limit and Hilbert expansions in the moment equations. After setting up the model, we perform several numerical tests to study the role of the local characteristics and the extended generator of the PDifMP in the process of tumour progression. The main aim focuses on understanding how the variations of the jump rate function of this process at the microscopic scale and the diffusion coefficient at the macroscopic scale are related to the diffusive behaviour of the glioma cells and to the onset of malignancy, i.e., the transition from low-grade to high-grade gliomas.

Keywords Piecewise diffusion Markov process · Stochastic modelling for cell motion · Low grade glioma model · Onset of malignancy

Martina Conte and Amira Meddah have contributed equally to this work.

✉ Amira Meddah
amira.meddah@jku.at

Evelyn Buckwar
evelyn.buckwar@jku.at

Martina Conte
martina.conte@polito.it

1 Institute of Stochastics, Johannes Kepler University, Altenberger Straße 69, 4040 Linz, Austria

2 Centre for Mathematical Sciences, Lund University, 221 00 Lund, Sweden

3 Department of Mathematical Sciences "G. L. Lagrange", Politecnico di Torino, Corso Duca degli Abruzzi 24, 10129 Torino, Italy

1 Introduction

Gliomas are the most common type of primary brain tumours, accounting for 78% of all malignant brain neoplasia.[1] They originate from mutations of the glial cells in the central nervous system and are classified by the World Health Organisation (WHO) into four grades according to the degree of malignancy [see (Wesseling and Capper 2018)] for a more detailed description). In this work, we mainly focus on low grade gliomas (LGGs), which are a class of rarely curable diseases, often resulting in the premature death of the patient. Since in the last years some medical interventions have been shown to improve the median survival time of patients, the study of this class of tumour has become of great importance for the clinicians.

The development, growth, and invasion of gliomas in the brain is a very complex phenomenon, involving many interrelated processes over a wide range of spatial and temporal scales. As such, often the individual cell behaviours and the intracellular dynamics described at a microscopic scale are manifested by functional changes in the cellular and tissue level phenomena. Therefore, this multiscale nature of glioma evolution requires modelling techniques that are able to deal with different levels of description.

The first mathematical models for the study of brain tumours started to emerge in the early 1980s (see (Düchting and Dehl 1980; Düchting and Vogelsaenger 1981, 1985; Tracqui et al. 1995; Tracqui 1995) for further details). Since then, the mathematical modelling of glioma evolution has evolved considerably and several different approaches have been proposed, going from discrete or hybrid microscopic models to macroscopic and multiscale frameworks. Discrete models at the microscopic scale, also called agent-based models, have been used to describe the dynamics of individual cells moving on a lattice (for some examples we refer the reader to (Wang et al. 2015; Metzcar et al. 2019; Hatzikirou et al. 2012), or, specifically, to Aubert et al. (2006) for cellular automata models and Gao et al. (2013) for cellular Potts models). Further, stochastic discrete models for cell motion have also been proposed, e.g. describing 2D persistent random walk or 3D anomalous diffusion (Dunn and Brown 1987; Luzhansky et al. 2018; Audoin et al. 2022; Scott et al. 2021). In particular, recently in Scott et al. (2021), the authors have presented the analysis of 3D cell tracking data, based on a persistent random walk model adapted into the context of glioma cell migration. At the macroscopic scale, several phenomenological models for glioma evolution stated in the form of reaction-diffusion-advection equations have been proposed and studied (Swanson et al. 2003; Harpold et al. 2007; Tracqui et al. 1995; Swanson et al. 2000), also including patient-specific data (e.g. in the form of diffusion tensor imaging (DTI) information). We refer for example to Swan et al. (2018), where the authors performed a series of in silico simulations in which their anisotropic model is fitted to 10 patient data, showing a slight improvement over the standard Proliferation-Infiltration (PI) model introduced in Swanson et al. (2000). This has allowed for a comparison between the real and the virtual tumour evolution (Jbabdi et al. 2005; Konukoglu et al. 2010; Clatz et al. 2005; Mosayebi et al. 2012). Concerning multiscale models,

[1] Information available at https://www.aans.org/en/Patients/Neurosurgical-Conditions-and-Treatments/Brain-Tumors

a broad and rich literature has been developed for the integration of microscopic and macroscopic dynamics (for some examples see (Hillen 2006; Hillen and Painter 2013; Bellomo et al. 2012; Painter and Hillen 2013; Engwer et al. 2015, 2016a; Lorenz and Surulescu 2014; Kelkel and Surulescu 2012; Engwer et al. 2016b)). In particular, in Engwer et al. (2015), a more detailed description of the migration process of individual cells, involving the dynamics of cell receptors and the interaction with the tumour microenvironment, is discussed.

A key aspect of modelling tumour evolution concerns cell movement, which is based on a combination of complex processes involving motility and migration: motility refers to the random movement from one location to another, while migration involves also the interactions between cells and the microenvironment.[2]

The first description of particle movement, which uses a stochastic Markov process combining deterministic ordinary differential equations (ODEs) for the continuous movement with Poisson-like jumps for the random change of direction, was introduced in 1974 by Stroock (1974) on the basis of the biological observations illustrated in Adler (1966). The concept of piecewise deterministic Markov processes (PDMPs) was introduced in 1984 in Davis (1984). An extension of Davis (1984) was then provided in Bujorianu and Lygeros (2004, 2006), where the authors developed the extended generator and the differential formula for piecewise diffusion Markov processes (PDifMPs), showing that all the classes of proposed stochastic hybrid processes can be seen as a special case of their concept of a general stochastic hybrid system (GSHS). Further, in Blom (1988) a general class of continuous-time stochastic hybrid systems, in which the continuous flow is the solution flow of a stochastic differential equation (SDE), was presented. These processes have been widely applied in different contexts, e.g. for interacting particle systems (Blom et al. 2018), air traffic management (Bujorianu and Lygeros 2005), or gene network (Nankep et al. 2018)) and especially in biological modelling [for some examples, see (Uatay 2019; Fontbona et al. 2010; Cloez et al. 2017; Pakdaman et al. 2010; Genadot and Thieullen 2014; Riedler 2011; Crudu et al. 2012; Rudnicki and Tyran-Kamińska 2017)]. However, it seems that the use of PDifMPs in the context of tumour growth, motility, and migration has not yet been investigated. Therefore, in this article we extend the description of cell movement based on velocity jump processes with the use of PDifMPs in the context of glioma progression. With respect to the previously proposed approaches, we provide a clear distinction between cell motility and migration. Moreover, we apply the proposed approach to the study of a novel aspect concerning the transition to malignancy of the tumour mass by analysing its relationship with specific model features (e.g., cell turning rate and diffusion coefficient). Precisely, we build a multiscale model, starting with a contact-mediated description of cell motion on the microscopic scale using PDifMPs. We then use the extended generator for such processes to derive a generalised Fokker–Planck equation, used as the basis for our model and including the description of the tumour-microenvironment interactions. The solution of the proposed equation provides the joint density of the transition probabilities of this Markov process for all the involved variables. As the variables involved in these interactions are fast-acting compared to the macroscopic scale, we make use of a scale separation

[2] Information available at https://phiab.com/applications/cell-motility-and-migration

variable and the Hilbert expansion method to derive the corresponding macroscopic scale equation for the time and space variables (for a more general discussion of multiscale modelling and moment closure techniques, we refer the reader to Bhattacharya et al. (2021), Kuehn (2016), Hunt (2018)).

The paper is organised as follows. Section 2 contains a brief introduction to PDifMPs. In Sect. 3, we derive a stochastic multiscale model for glioma progression. Numerical simulations in a 2D scenario for the resulting macroscopic equation for the tumour cell density are presented in Sect. 4, including several studies on the effect of parameter variations. Finally, in Sect. 5, we review our results and discuss further directions of research.

2 Preliminaries on PDifMPs

2.1 Definition and notation

In this section, we provide a brief introduction to PDifMPs and the construction of their paths. We refer the reader to Bujorianu and Lygeros (2006) and Nankep et al. (2018) for a general description of stochastic hybrid systems.

Let $(\Omega, \mathcal{F}, (\mathcal{F})_{t\geq 0}, \mathbb{P})$ be a filtered probability space and $(W_t)_{t\in[0,T]}$ an m-dimensional standard Wiener process, with $m \in \mathbb{N}$ and $T > 0$. We consider the PDifMP defined by $(U_t)_{t\in[0,T]} := \{U(t,\omega), t \in [0,T], \omega \in \Omega\}$. It consists of two different components, i.e., $U_t = (S_t, V_t)$ with values in $E = E_1 \times \mathbf{V}$. In particular, $E_1 \subset \mathbb{R}^{d_1}$ and $\mathbf{V} \subset \mathbb{R}^{d_2}$, with $d_1, d_2 \in \mathbb{N}$ and E endowed with the Borel algebra $\mathcal{B}(E)$. The closure of the set E is denoted by $\bar{E}$, while ∂E stands for its boundary.

For the couple of non-exploding processes (S_t, V_t), we assume that the first stochastic component $(S_t)_{t\in[0,T]}$ possesses continuous paths in E_1 and the second component $(V_t)_{t\in[0,T]}$ is a jump process with right continuous paths and piecewise constant values in $\mathbf{V}$. The times $(T_i)_{i\in\mathbb{N}}$ at which the second component jumps form a sequence of randomly distributed grid points in $[0,T]$. The motion of the PDifMP $(U_t)_{t\in[0,T]}$ on $(E, \mathcal{B}(E))$ is defined by its characteristic triple $(\phi, \lambda, \mathcal{Q})$ as follows:

- $\phi : [0,T]\times E \to E_1, (t,u) \mapsto \phi(t,u)$, is the stochastic flow of the continuous first component of $(U_t)_{t\in[0,T]}$. Starting at $T_0 = 0$ with initial value $u_0 = (s_0, v_0) \in E$, the process $\phi(t,u)$ represents the solution of a sequence of SDEs over the consecutive intervals $[T_i, T_{i+1})$ of random length. At each random point $T_i \in [0,T]$, $i \geq 1$, there are newly updated initial values $u_i = (s_i, v_i) \in E$, where s_i serves as the initial value and v_i as a parameter in the following SDE defined on the interval $[T_i, T_{i+1})$:

$$\begin{cases} d\phi(t,u_i) = b(\phi(t,u_i), v_i)dt + \sigma(\phi(t,u_i), v_i)dW_t, & t \in [T_i, T_{i+1}), \\ \phi(T_i, u_i) = s_i. \end{cases} \tag{1}$$

  At the endpoint T_{i+1} of each interval, s_{i+1} is set to the current value of $\phi(\cdot, u_i)$ to ensure the continuity of the path. Further, a new value v_{i+1} is chosen as fixed parameter for the next interval according to the jump mechanism described below.

We define also the function b with values in $\mathbb{R}^{d_1}$, which represents a family of drift coefficients, and the $d_1 \times m$ matrix σ with real coefficients.

Assumption 1 We assume that $b : E \to \mathbb{R}^{d_1}$ and $\sigma : E \to \mathbb{R}^{d_1 \times m}$ are linearly bounded and globally Lipschitz continuous for all $s \in E_1$.

For any $v_i \in \mathbf{V}$, this assumption ensures the existence and uniqueness of the solution to (1) (see Theorem 5.2.1 in Oksendal (2013)). Moreover, the stochastic flow satisfies the semi-group property, i.e.,

$$\phi_{v_i}(t+\delta, \cdot) = \phi_{v_i}(t, \phi_{v_i}(\delta, \cdot)), \qquad \forall t, \delta \in [0, T].$$

- $\lambda : E \to \mathbb{R}_+$ is the jump rate, i.e, it determines the frequency at which the second component of $(U_t)_{t\in[0,T]}$ jumps.
- $\mathcal{Q} : (E, \mathcal{B}(E)) \to [0, 1]$ is the transition kernel that determines the new values of the second component after a jump occurs. For all $u \in E$, it satisfies $\mathcal{Q}(u, \{u\}) = 0$, meaning that the process cannot have a no-move jump.

Moreover, for all $t \in [T_i, T]$, $i \geq 0$, we define the survival function of the inter-jump times as

$$\mathcal{S}(t, u_i) := \exp\left(-\int_{T_i}^{t} \lambda(\phi(\delta, u_i), v_i) d\delta\right), \qquad u_i \in E. \tag{2}$$

This function states that there is no jump in the time interval $[T_i, t)$ conditional on the process being in the initial state u_i. Let $\mathcal{U}$ be a uniformly distributed random variable on $[0, 1]$, thus $\zeta : [0, 1] \times E \to \mathbb{R}_+$ is the generalised inverse of $\mathcal{S}(t, u_i)$ defined by

$$\zeta(\mathcal{U}, u_i) = \inf\{t \geq 0 ; \mathcal{S}(t, u_i) \leq \mathcal{U}\}.$$

Assumption 2 Let $\lambda : E \to \mathbb{R}_+$ be a measurable function such that $\forall u_i \in E$ and $T > 0$

$$\int_0^T \lambda(\phi(t, u_i), v_i) dt < \infty \quad \text{and} \quad \int_0^\infty \lambda(\phi(t, u_i), v_i) dt = \infty. \tag{3}$$

Moreover, there exists a measurable function $\psi : [0, 1] \times E \to E$ such that for $u_i \in E$ and $B \in \mathcal{B}(E)$

$$\mathbb{P}(\psi(\mathcal{U}, u_i) \in B) = \mathcal{Q}(u_i, B).$$

ψ represents the generalised inverse function of $\mathcal{Q}$. For a fixed t, $\psi(\mathcal{U}(\omega), U(\omega))$ is a random variable describing the post-jump locations of the second component of U.

Assumption 3 For all $B \in \mathcal{B}(E)$, $\mathcal{Q}(\cdot, B)$ is measurable, while for all $u \in \bar{E}$ the function $\mathcal{Q}(u, \cdot)$ is a probability measure.

Summarising, the first component of the triple $(\phi, \lambda, \mathcal{Q})$ describes the continuous evolution of the trajectories of the process $(U_t)_{t\in[0,T]}$ between jumps in time intervals defined by the survival function $\mathcal{S}$, while the couple $(\lambda, \mathcal{Q})$ yield the jump mechanism. All three components of $(\phi, \lambda, \mathcal{Q})$ are coupled.

2.2 Construction

From the local characteristics $(\phi, \lambda, \mathcal{Q})$, it is possible to iteratively construct the sample path U_t as follows. Let $(\mathcal{U}_n)_{n\geq 1}$ be a sequence of iid random variables with uniform distribution on [0, 1] and $u_0 = (s_0, v_0) \in E$ the initial value of (1) at $T_0 = 0$, such that u_0 can be either an $\mathcal{F}_0$-measurable random variable (independent from the Wiener process) or a deterministic constant, for some $\omega \in \Omega$. We apply the survival function $\mathcal{S}(t, u_0)$ defined in (2) and use its generalised inverse ζ with the first element $\mathcal{U}_1$ to determine $T_1 = \zeta(\mathcal{U}_1, u_0)$, i.e., the first jump time of the second component of U_t. We then define the sample path U_t up to the first jump time as

$$\begin{cases} U_t = \phi(t, u_0) & \text{for } 0 \leq t < T_1, \\ U_{T_1} = \psi\left(\mathcal{U}_2, \left(\phi(T_1, u_0), v_0\right)\right). \end{cases}$$

The trajectory of U_t follows the stochastic flow ϕ given in (1) starting from $U_0 = u_0$ until a first jump occurs at the random time $t = T_1$. The post-jump state U_{T_1} is determined through the measurable function ψ. For all $B \in \mathcal{B}(E)$, the distribution of $\psi(\mathcal{U}_2, u_0)$ is given by

$$\mathbb{P}(V_{T_1} \in B | t = T_1, S_0 = s_0) = \mathcal{Q}\left((\phi(\tau_1, u_0), v_0), B\right), \tag{4}$$

where τ_1 is the waiting time until the first jump occurs, i.e. $\tau_1 = T_1$.

Restarting the process from the post-jump location U_{T_1}, we define

$$\tau_2 = \zeta(\mathcal{U}_3, U_{T_1})$$

the next waiting time before a jump occurs from the survival function (2). In this way, we find the next jump time $T_2 = T_1 + \tau_2$.

Consequently, the state of the process in the interval $[T_1, T_2)$ is given by

$$\begin{cases} U_t = \phi(t - T_1, U_{T_1}) & \text{for } \quad T_1 \leq t < T_2, \\ U_{T_2} = \psi\left(\mathcal{U}_3, \left(\phi(\tau_2, (U_{T_1}, v_0)), v_0\right)\right). \end{cases}$$

We proceed recursively to obtain a sequence of jump times $(T_i)_{i\geq 1}$,

$$T_i = T_{i-1} + \zeta(\mathcal{U}_{2i-1}, U_{T_{i-1}}) \qquad \forall\, i \geq 1,$$

such that the generic sample path of U_t, for $t \in [T_i, T_{i+1})$, is defined accordingly by

$$\begin{cases} U_t = \phi(t - T_i, U_{T_i}) & \text{for} \quad T_i \le t < T_{i+1}, \\ U_{T_{i+1}} = \psi\left(\mathcal{U}_{2i+2}, \left(\phi(\tau_{i+1}, (U_{T_i}, v_{i+1})), v_{i+1}\right)\right). \end{cases}$$

The number of jump times that occur between 0 and t is denoted by

$$N_t = \sum_{i \ge 1} \mathbb{1}_{(T_i \le t)}.$$

Assumption 4 For all $t > 0$ and for every starting point $u_i \in E$, $\mathbb{E}[N_t | u = u_i] < \infty$.

This assumption ensures the non-explosion of the process U_t. Under the Assumptions 1-4 the piecewise diffusion process can be constructed as a strong càdlàg Markov process [see (Bujorianu and Lygeros 2006) for further details], called then a Piecewise Diffusion Markov Process (PDifMP).

2.3 Extended generator of the PDifMP

The notion of infinitesimal generator is an extremely important tool for the study of Markov processes (Bielecki and Frankiewicz 2006; Davis 1984). In the following, we adopt the definition in (Nankep et al. 2018; Bujorianu and Lygeros 2006), and, for the reader's convenience, we recall the theorem that fully characterised the extended generator [see (Bielecki and Frankiewicz 2006) and references therein for further details about the difference between extended and classic generators].

Theorem 1 *Let U_t be a PDifMP with characteristics $(\phi, \lambda, \mathcal{Q})$. The domain $\mathcal{D}(\mathcal{A})$ of the extended generator $\mathcal{A}$ consists of all bounded, measurable functions f on $E \cup \partial E$ satisfying:*

1. *$f : \bar{E} \to \mathbb{R}$ $\mathcal{B}$-measurable such that $s \mapsto f(s, v)$ is a.e $C^2(\bar{E})$,*
2. $$f(u) = \int_E f(y)\mathcal{Q}(u, dy), \ u \in \partial E,$$
3. *$Bf \in L_1^{loc}(p)$ where*
$$Bf(u, t, \omega) := f(u) - f\left(u_{t-}(\omega)\right).$$

Then, for $f \in \mathcal{D}(\mathcal{A})$, $u = (s, v) \in E$, the extended generator $\mathcal{A}f$ is given by

$$\mathcal{A}f(s, v) = \mathcal{A}_{dif} f(s, v) + \lambda(s, v) \int_E (f(s, \xi) - f(s, v))\mathcal{Q}((s, v), d\xi), \qquad (5)$$

where

$$\mathcal{A}_{dif} f(s,v) := \sum_{i=1}^{d_1} b_i(s,v)\partial_i f(s,v) + \frac{1}{2}\sum_{i,j=1}^{d_1} (\sigma\sigma^T)_{ij}(s,v)\partial_i\partial_j f(s,v),$$
$$= \nabla_s f(s,v)\cdot b(s,v) + \frac{1}{2}\mathrm{Tr}[(\sigma\sigma^T)(s,v)(\nabla_s\nabla_s^T) f(s,v)], \qquad (6)$$

for $s = (s_1, \ldots, s_{d_1})$. *Here,* $\nabla_s f(s,v)\cdot b(s,v)$ *is the inner product in* $\mathbb{R}^{d_1}$, σ^T *is the transpose matrix of* σ *and* ∇_s^T *is the transpose operator of* ∇_s. *Precisely,*

$$(\sigma\sigma^T)(s,v)(\nabla\nabla^T) f(s,v) = \left(\sigma_i\sigma_j\partial_i\partial_j f(s,v)\right)_{i,j=1\ldots d_1}.$$

We refer to Bujorianu and Lygeros (2006) for the definition of $L_1^{\mathrm{loc}}(p)$ and the proof of this theorem.

2.4 Generalised Fokker–Planck equation

The adjoint of the generator is used to derive the generalised Fokker–Planck equation, describing the time evolution of the probability distribution $g(t,s,v)$ of the process. The equation is given by

$$\partial_t g(t,s,v) = \mathcal{A}^*_{\mathrm{dif}} g(t,s,v) + \lambda(s,v)\int_E (g(s,\xi) - g(s,v))\mathcal{Q}((s,v),d\xi), \qquad (7)$$

where the adjoint operator of $\mathcal{A}_{\mathrm{dif}}$ reads

$$\mathcal{A}^*_{\mathrm{dif}} g(t,s,v) = -\nabla_s\left(b(s,v)g(t,s,v)\right) + \frac{1}{2}\mathrm{Tr}\left[\left(\nabla_s\nabla_s^T\right)\left(\sigma\sigma^T(s,t)g(t,s,v)\right)\right]. \qquad (8)$$

We refer to Bect (2007), Gardiner (1985) for further details on the derivation of Fokker–Planck equations for general Markov processes.

3 Application to tumour modelling

Gliomas can be considered as dynamical ecosystems where cells undergo constant changes due to many cellular processes, e.g. migration, proliferation, death, or creation of new blood vessels (Tamai et al. 2022; Ahir et al. 2020). We focus on the process of cell movement, which is responsible for the global diffusive features that characterise glioma evolution. Cell movement can be divided into motility and migration. Motility refers to the random or spontaneous motion of cells from one location to another, while cell migration involves many interconnected biological aspects, such as environmental cues driving it. Thus, methods that take into consideration the stochastic nature of this phenomenon (i.e., motility) while accounting for environmental cues influencing it

(i.e., migration) are important for providing a more complete understanding of the entire process.

Following (Kelkel and Surulescu 2012; Hunt 2018), we model the process of cell movement under the influence of subcellular scale interactions taking into account the effects of the amount of bound receptors located on the cell membrane. More precisely, we consider the role of these receptors, referring to them as integrins in this dynamics. n fact, integrins have been shown to play a significant role in facilitating the infiltration of tumor cells through normal brain tissue, and are considered a major contributor to the invasive glioma phenotype (Demuth and Berens 2004) and a key regulator of glioma cell migration (Paulus et al. 1996; Tonn et al. 1998). Regarding cell migration, we consider tissue alignment as an important cue enhancing the efficiency of cell invasion (Demuth and Berens 2004; Tonn et al. 1998). In fact, even if the exact interactions of glioma cells with white matter tracts is largely unknown, it has been shown that glioma do follow white matter tracts (Giese et al. 1996; Giese and Westphal 1996; Giovanna and Kaye 2007), attaching to the fibers and crawl along them, a phenomenon at least partially attributed to the complex involvement of integrin dynamics. However, since the direction that cells decide to follow remains random, there is a need to consider a stochastic description for the motility component.

Inspired by particle movement models (Stroock 1974; Othmer and Hillen 2000, 2002), we propose piecewise diffusion Markov processes for the modelling of cell movement. In the context of persistent random motion, the continuous stochastic component of the PDifMP describes the migration phenomenon, while its second component describes the random motility dependent on the velocity jump process. This approach makes it possible to describe the cellular migratory response to environmental signals while keeping the random aspect of cell motility. Moreover, it also allows us to show how several well-established methods proposed in the literature (e.g. see (Othmer and Hillen 2000, 2002; Hunt 2018)) can be cast into a rigorous PDMP framework.

3.1 Microscopic scale

3.1.1 Interactions between cells and microenvironment

In order to migrate through the complex structures of the brain, glioma cells must adapt to the physical characteristics of the environment. Their interactions with the extracellular matrix (ECM) Frantz et al. (2010) are mediated by the binding between integrins and ECM proteins. These binding processes are, in fact, involved in cell motility and migration, and they also affect cell growth, division, and proliferation. Considering the migration phenomenon, several experiments show that these bindings allow cells to exert the forces necessary for their migration (see Demuth and Berens 2004 and references therein). As these processes occur at the subcellular level, we describe the mechanism behind cell movement modelling the dynamics of receptors on the tumour cell membrane.

Let $y(t)$ be the concentration of bound integrins and let us assume that the binding between integrins and tissue occurs in areas of highly aligned fibers (Engwer et al. 2015). The binding process can be described with the following general reaction

$$A + (R_0 - y) \underset{k^-}{\overset{k^+}{\rightleftharpoons}} y \tag{9}$$

where R_0 defines the total number of cell surface receptors, $A(x)$ the macroscopic volume fraction of tissue (including ECM and brain fibers), depending on the position $x \in \mathbf{X} \subset \mathbb{R}^3$, and k^+ and k^- the rates of attachment and detachment between cell and tissue (Engwer et al. 2015, 2016b). Within this framework, denoting by $x = x_0 + vt$, we look at the path of a single cell moving from an initial position x_0 with velocity $v \in \mathbf{V} \subset \mathbb{R}^3$. $\mathbf{V} = \alpha\mathbb{S}^2$ is the closed set for cell velocities, where $\mathbb{S}^2$ denotes the unit sphere on $\mathbb{R}^3$ and α the mean speed of a tumour cell, which is assumed to be constant. Since we are interested in the interactions between cell surface receptors and the ECM, and this binding process takes place for fixed position x, we ignore any type of randomness resulting from the velocity change. The mass action kinetics for the concentration $y(t)$ is governed by the following ODE:

$$\frac{dy}{dt} = k^+(R_0 - y)A(x) - k^- y. \tag{10}$$

Since the averaged subcellular dynamics of integrin receptor binding happens very fast in comparison to the evolution of cells and tissue, i.e., with respect to the macroscopic time scale, we assume that it equilibrates rapidly (Engwer et al. 2016a; Hunt 2018; Conte 2021). Thus, we first rescale $y/R_0 \to y$, such that here $y(t) \in (0, 1)$, and then we consider the unique steady state y^* of (10), given by

$$y^* = \frac{k^+A(x)}{k^+A(x) + k^-} =: f(A(x)), \tag{11}$$

To better understand the variation of y around its steady state, we introduce a new internal variable $z = y - y^*$ with values in the interval $\mathbf{Z} = (y^* - 1, y^*)$. This allows us to measure the deviation of y from its steady state and study how it varies in the neighborhood of y^* (Engwer et al. 2015; Hunt 2018). Considering the piecewise location of a single cell $x = x_0 + vt$ through the density field $A(x)$, z satisfies

$$\frac{dz}{dt} = -\Big(\underbrace{(k^+A(x) + k^-)z - f'(A(x))\langle v, \nabla_x A(x)\rangle}_{:=G(t,x,v,z,A)} \Big), \tag{12}$$

where $\langle \cdot, \cdot \rangle$ is the scalar product on $\mathbf{V} \times \mathbb{R}^3$ and $f'(A(x)) = \frac{k^+k^-}{(k^+A(x)+k^-)^2}$. The internal variable z is bounded as long as $\nabla_x A(x)$ is bounded and its sign depends on the current orientation of the cell w.r.t the gradient of $A(x)$.

3.1.2 PDifMP description for glioma cell movement

To model cell movement under the influence of external signals, we assume that the sample path of an individual cell starting in position x_0 and moving in a certain direction due to contact guidance for a random period of time is given by

$$\begin{cases} dx_t &= v_t dt + \sigma dW_t, \\ x(0) &= x_0. \end{cases} \tag{13}$$

Here, the second term in the r.h.s represents the stochastic variability in the velocity, with $\sigma \in \mathbb{R}$ being the constant diffusion coefficient and W_t the standard Wiener process.

Due, for instance, to collisions with other cells in their surrounding (Loy and Preziosi 2020; Painter and Hillen 2002), during the movement a cell stops for a negligible duration and reorients its path (Loy and Preziosi 2020). This causes the cell to adopt a new velocity to continue migrating in the new direction until another obstacle is encountered. To describe this process, we rely on the introduced PDifMP framework. We set $E_1 = \mathbf{X} \times \mathbf{Z} \subset \mathbb{R}^4$ and we denote by $S_t := (X_t, Z_t)$ the continuous component describing cell motion. Their evolution is characterised through the SDE (13) for cell motility and the ODE (12) for the interactions with the microenvironment. Both processes are affected by spontaneous velocity changes induced by the jump process V_t. Then, we denote by $E = E_1 \times \mathbf{V}$ the state space of the piecewise process $U_t = (X_t, Z_t, V_t)$ for cell motility and migration and by $\phi : [0, T] \times E \to E_1$, the solution to the coupled system (12)–(13).

Under the assumption that the duration of reorientation is negligible, it is possible to talk about the direction of a cell at a given instant. Moreover, under the additional assumption that the motion is Markovian in the state space, we state that cell direction is described with an inhomogeneous Poisson-like process (Gabbiani and Cox 2017), whose intensity depends on time, position on the scaled sphere $\mathbf{V}$, and internal state. Thus, the cell reorientation rate referring to the jump rate function $\lambda : [0, T] \times E \to \mathbb{R}_+$ of the stochastic process u_t depends on the integrin state z. This means that the binding process is seen as the onset of reorientation. In particular, following (Sun et al. 2006), we assume that, if many integrins are bounded, cells tend to change direction frequently in order to escape the densely packed areas, resulting in an increased rate λ. Thus, following (Engwer et al. 2016a, b), we set $\lambda(u_t) := (\lambda_0 - \lambda_1 z_t) \geq 0$, with $\lambda_0 > 0$ and λ_1 constant parameters. In particular, λ_0 refers to the basal turning frequency of an individual cell (Sidani et al. 2007) accounting for the "spontaneous" cell motility, while the term $\lambda_1 z$ represents the variation of the turning rate in response to environmental signals.

Following the construction described in Sect. 2.2 with initial state $u_0 = (x_0, z_0, v_0)$, we use the jump rate function λ defined in (2) to determine the duration of movement before any reorientation of direction occurs. Moreover, considering that the velocity jump process v_t is of Markovian type, we have that cells retain no memory of their velocities before the reorientation. Thus, we define the Markov transition kernel $\mathcal{Q}(x, dv)$, determining a post-velocity jump state v' of the process u_t, given that the process was in the state v before the jump. This describes in this context the distribution of newly chosen velocities.

Definition 1 Let ν be the standard Lebesgue measure on $(\mathbf{V}, \mathcal{V})$ and $K : \mathbf{X} \times \mathbf{V} \to [0, \infty]$ be a measurable function with respect to the σ-algebra $\mathcal{X} \otimes \mathcal{V}$ such that

$$\int_{\mathbf{V}} K(x, v)\nu(dv) = 1, \quad \forall x \in \mathbf{X}. \tag{14}$$

Then, the mapping

$$\begin{cases} \mathcal{Q} : \mathbf{X} \times \mathcal{V} \to [0, 1], \\ \mathcal{Q}(x, B) = \int_B K(x, v)\nu(dv), \end{cases}$$

defines a Markov kernel over $\mathbf{V}$, where $\nu(dv) = dv$. Note that $\mathcal{Q}(x, \cdot)$ is a probability measure on $(\mathbf{V}, \mathcal{V})$ for each $x \in E$, since

$$\mathcal{Q}(x, \mathbf{V}) = \int_{\mathbf{V}} K(x, v)dv = 1.$$

To define the kernel function K, we introduce the fiber distribution function $q(x, \hat{v})$ over $\mathbf{V}$, with $\hat{v} = \frac{v}{\|v\|} \in \mathbb{S}^2$, and

$$w := \int_{\mathbf{V}} q(x, \hat{v})dv = \alpha^2,$$

a scaling constant (Hillen and Painter 2013; Hillen 2004), we assume that the dominant directional cue leading cell migration is given by the fiber network. Thus, the the kernel function K is given by

$$K(x, v) = \frac{q(x, \hat{v})}{w}. \tag{15}$$

For the fiber distribution function $q(x, \hat{v})$, different expressions can be found in the literature, such as the Von Mises-Fisher Distribution, the Peanut Distribution Function, or the Orientation Distribution Function (ODF) (Painter and Hillen 2013; Aganj et al. 2011). A comparison among these distributions has been proposed in Conte et al. (2020), in both 1D and 2D scenarios. We rely on this analysis and we choose the ODF for describing $q(x, \hat{v})$, i.e., we set

$$q(x, \hat{v}) = \frac{1}{4\pi \mid \mathbb{D}(x) \mid^{\frac{1}{2}} (\hat{v}^T (\mathbb{D}(x))^{-1} \hat{v})^{\frac{3}{2}}}. \tag{16}$$

Here, $\hat{v}$ stands for the fiber direction, x for the spatial position within the brain, while $\mathbb{D}$ is the diffusion tensor taking into account information about the water diffusivity in the brain (Conte et al. 2020). We also assume that fibers are not polarised, i.e., $q(x, \hat{v}) = q(x, -\hat{v})$ for all $\hat{v} \in \mathbb{S}^2$. It is straightforward to verify that q is a probability distribution on $\mathbb{S}^2$ (Engwer et al. 2015, 2016a, b).

From (2), it is possible to construct the sequence of jump times $(T_n)_{n\geq 1}$, with $T_n = \tau_1 + \cdots + \tau_n$ for all $n \geq 1$ (and $T_0 = 0$ by convention), such that the process U_t describing cellular movement is piecewise constructed on each interval $[T_i, T_{i+1})$, $i = 1, \ldots, n$, via the characteristics $(\phi, \lambda, \mathcal{Q})$ given by

$$\begin{cases} \phi &= (v_t t + \sigma W_t, z_t)^T, \\ \lambda &= \lambda_0 - \lambda_1 z_t, \\ \mathcal{Q} &= \dfrac{1}{w} \displaystyle\int_{\mathbf{V}} q(x, \hat{v})dv. \end{cases} \tag{17}$$

Here, z_t is the solution of (12) and v_t is a piecewise constant over each interval of random length $T_{i+1} - T_i$. As proven in Bujorianu and Lygeros (2006), this construction leads to a càdlàg strong Markov process, describing cell motion in an anisotropic environment.

Given initial values (X_0, Z_0, V_0) at T_0, the system describing a contact-mediated movement of glioma cells at the microscopic scale is thus a system concatenated over all subsequent intervals $[T_i, T_{i+1})$, such that for all $t \in [T_i, T_{i+1})$, $i \geq 0$, we have

$$\begin{cases} dX_t = V_t dt + \sigma dW_t, \\ dZ_t = -\big(G(t, X_t, Z_t, V_t, A)\big)dt, \\ dV_t = 0dt, \end{cases} \tag{18}$$

with initial values at the jump time T_i given by the values of X_t and Z_t at the endpoint of the previous interval and a new constant value for V_t drawn from the transition kernel $\mathcal{Q}$. The overall process of concatenated solutions of (18) is a triple $U_t = (X_t, Z_t, V_t) \in E$, with $E = E_1 \times \mathbf{V} = (\mathbb{R}^3 \times \mathbb{R}) \times \alpha\mathbb{S}^2$. Hereafter we will refer to (X_t, Z_t, V_t) as (x_t, z_t, v_t) as we are talking about the sample path of U_t.

3.2 Derivation of the mesoscopic equation and its macroscopic limit

We start from the definition of the extended generator of $(U_t)_{t\in[0,T]}$ given in Sect. 2.3, where the solution $g(t, x, z, v)$ is the joint density function of the microscopic stochastic process variables X, Z and V at time $t \in [0, T]$, for values of the position $x \in \mathbf{X}$, internal state $z \in \mathbf{Z}$, and velocity $v \in \mathbf{V}$. We interpret the function $g(t, x, z, v)$ as the mesoscopic description for the tumour cell distribution. Further, for all test functions $f \in \mathcal{D}(\mathcal{A})$, the extended generator $\mathcal{A}$ of the above defined process U_t reads

$$\begin{aligned} \mathcal{A}f(x, z, v) = &\langle \nabla_s f(x, z, v), b(x, z, v)\rangle \\ &+\frac{1}{2}\sigma^2 \operatorname{Tr}\left((\nabla_x \nabla_x^T) f(x, z, v)\right) + \lambda(z) \int_{\mathbf{V}} (f(x, z, v') \\ &- f(x, z, v))\mathcal{Q}(x, v, dv'). \end{aligned} \tag{19}$$

Here $s = (x, z)$, $b(x, z, v) = (v_1, v_2, v_3, -G(x, z, v, A), 0, 0, 0)$, λ and $\mathcal{Q}$ is given in (17). Notice that the integral term in (19) is defined over $\mathbf{V}$ as the transition kernel $\mathcal{Q}$ has a density defined on $\mathbf{V}$. The adjoint operator $\mathcal{A}^* g$ is given by

$$\begin{aligned} \mathcal{A}^* g(t, x, z, v) = &-\big(\langle \nabla_x g(t, x, z, v), v\rangle - \partial_z \left(G(t, x, z, v, A) g(t, x, z, v)\right)\big) \\ &+\frac{1}{2}\sigma^2 \operatorname{Tr}\left((\nabla_x \nabla_x^T) g(t, x, z, v)\right) \\ &+\lambda(z) \int_{\mathbf{V}} (g(t, x, z, v') - g(t, x, z, v))\mathcal{Q}(x, v, dv'). \end{aligned} \tag{20}$$

Thus, following the analysis of Sect. 2.4, the generalised Fokker–Planck equation for the evolution of $g(t, x, z, v)$ reads

$$\partial_t g(t,x,z,v) + \langle \nabla_x g(t,x,z,v), v\rangle - \partial_z \left(G(t,x,z,v,A) g(t,x,z,v)\right)$$
$$-\frac{1}{2}\sigma^2 \operatorname{Tr}\left((\nabla_x \nabla_x^T) g(t,x,z,v)\right) = \mathcal{L} g(t,x,z,v), \tag{21}$$

where, from (15), the turning operator reads (Othmer and Hillen 2000; Hillen 2005; Painter and Hillen 2013; Engwer et al. 2016a)

$$\mathcal{L} g(x,z,v) = \lambda(z) \int_{\mathbf{V}} (g(x,z,v') - g(x,z,v)) \frac{q(x,v)}{w} dv', \tag{22}$$

Remark 1 Note that for $\sigma = 0$, (21) coincides with the kinetic transport equation derived in (Engwer et al. 2016a; Hunt 2018; Engwer et al. 2015). This means that the PDMP resulting from setting $\sigma = 0$ in (21) is the formally defined mathematical model underlying the description in Engwer et al. (2016a), Hunt (2018), Engwer et al. (2015). This idea was first introduced in Stroock (1974), in the context of modelling bacterial motion.

Following (Engwer et al. 2016a; Hunt 2018), we now add at this mesoscopic level of the glioma model an appropriately mesoscopic proliferation term as an effect of cell-tissue interactions via integrin binding given by

$$\mathcal{P}(g(t,x,z,v)) = \mu(M(t,x)) \int_{\mathbf{Z}} \mathcal{X}(x,z,z') g(t,x,z',v) A(x) dz'. \tag{23}$$

Here, $M(t,x)$ denotes the macroscopic cell density, that is the marginal distribution of $g(t,x,z,v)$ over all possible velocities and internal states, i.e.,

$$M(t,x) = \int_{\mathbf{V}} \int_{\mathbf{Z}} g(t,x,z,v) dz dv.$$

Moreover, $\mu(M)$ is the growth function and the kernel $\mathcal{X}(x,z,z')$ is a probability density in the second variable z characterising the transition from z' to z during the proliferation process at position x. For $\mathcal{X}$, we only assume that the operator $\mathcal{P}(g)$ is uniformly bounded in the L^2-norm, a reasonable biological condition related to the space-imposed limits on cell division. Thus, for the evolution of the tumour cell distribution $g(t,x,z,v)$, we obtain the following equation

$$\partial_t g(t,x,z,v) + \langle \nabla_x g(t,x,z,v), v\rangle - \partial_z (G(t,z,A) g(t,x,z,v))$$
$$-\frac{1}{2}\sigma^2 \operatorname{Tr}\left((\nabla_x \nabla_x^T) g(t,x,z,v)\right) = \mathcal{L} g(t,x,z,v) + \mathcal{P}(g(t,x,z,v)). \tag{24}$$

For simplicity we keep the notation for g in (24), however, after adding the proliferation term (23) it is not the same joint probability density as in (21). We now introduce the notations

$$\mathbb{E}_q(x) := \int_{\mathbb{S}^2} \hat{v} q(x, \hat{v}) d\hat{v},$$
$$\mathbb{V}_q(x) := \int_{\mathbb{S}^2} (\hat{v} - \mathbb{E}_q) \otimes (\hat{v} - \mathbb{E}_q) q(x, \hat{v}) d\hat{v},$$

for the mean fiber orientation and the variance-covariance matrix of the fiber distribution, respectively. Notice that the symmetry on the fiber distribution implies $\mathbb{E}_q = 0$.

Due to the high dimensionality of (24), numerical simulations of this equation would be too expensive. Moreover, clinicians are more interested in the macroscopic dynamics of the tumour rather than in the lower scale interactions. Thus, we derive the macroscopic equation for the evolution of the tumour density, based on the definition of the moments of g with respect to v and z:

$$m(t, x, v) = \int_{\mathbf{Z}} g(t, x, z, v) dz \qquad M(t, x) = \int_{\mathbf{V}} m(t, x, v) dv$$
$$m^z(t, x, v) = \int_{\mathbf{Z}} z g(t, x, z, v) dz \qquad M^z(t, x) = \int_{\mathbf{V}} m^z(t, x, v) dv.$$

Notice that we do not consider higher order moments of g with respect to z as the subcellular dynamics are much faster than the events taking place on the other scales, so that the deviation z is close to zero.

Moreover, following (Engwer et al. 2015, 2016a), we consider a parabolic scaling of the moment equations setting $x \mapsto \epsilon x$ and $t \mapsto \epsilon^2 t$ for space and time variables, respectively. In particular, we scale the growth rate function $\mu(M)$ with ϵ^2 as it accounts for faster dynamics. Thus, dropping the (t, x) notation for simplicity, the rescaled moment equations read

$$\epsilon^2 \partial_t m + \epsilon \langle \nabla_x m, v \rangle - \epsilon^2 \frac{1}{2} \sigma^2 \operatorname{Tr}\left((\nabla_x \nabla_x^T) m \right) = -\lambda_0 m + \lambda_1 m^z + \lambda_0 \frac{q}{w} M$$
$$-\lambda_1 \frac{q}{w} M^z + \epsilon^2 \mu(M) \int_{\mathbf{Z}} \int_{\mathbf{Z}} \mathcal{X}(x, z, z') g(t, x, v, z') A(x) dz' dz. \tag{25}$$

and

$$\epsilon^2 \partial_t m^z + \epsilon \langle \nabla_x m^z, v \rangle - \epsilon^2 \frac{1}{2} \sigma^2 \operatorname{Tr}\left((\nabla_x \nabla_x^T) m^z \right) =$$
$$-(A(x) k^+ + k^-) m^z + \epsilon f'(A(x)) \langle v, \nabla_x A(x) \rangle m - \lambda_0 m^z + \lambda_0 \frac{q}{w} M^z$$
$$+\epsilon^2 \mu(M) \int_{\mathbf{Z}} \int_{\mathbf{Z}} z \mathcal{X}(x, z, z') g(t, x, v, z') A(x) dz' dz. \tag{26}$$

We consider the *Hilbert expansion methods* (Ellis 1973; Hunt 2018) expanding the moments of g as

$$m(t,x,v)=\sum_{k=0}^{\infty}\epsilon^k m_k\,, \qquad M(t,x)=\sum_{k=0}^{\infty}\epsilon^k M_k\,,$$
$$m^z(t,x,v)=\sum_{k=0}^{\infty}\epsilon^k m_k^z\,, \qquad M^z(t,x)=\sum_{k=0}^{\infty}\epsilon^k M_k^z.$$

By equating the same powers of ϵ in (25) and (26), we derive the equation for the leading order coefficient M_0 of the Hilbert expansion of M. Precisely,
ϵ^0:

$$0=-\lambda_0 m_0+\lambda_1 m_0^z+\lambda_0\frac{q}{w}M_0-\lambda_1\frac{q}{w}M_0^z \tag{27}$$
$$0=-(A(x)k^+ +k^-)m_0^z-\lambda_0 m_0^z+\lambda_0\frac{q}{w}M_0^z. \tag{28}$$

ϵ^1:

$$\langle\nabla_x m_0,v\rangle=-\lambda_0 m_1+\lambda_1 m_1^z+\lambda_0\frac{q}{w}M_1-\lambda_1\frac{q}{w}M_1^z \tag{29}$$
$$\langle\nabla_x m_0^z,v\rangle=-(A(x)k^+ +k^-)m_1^z+f^{'}(A(x))\langle v,\nabla_x A(x)\rangle m_0-\lambda_0 m_1^z+\lambda_0\frac{q}{w}M_1^z. \tag{30}$$

ϵ^2:

$$\partial_t m_0+\langle\nabla_x m_1,v\rangle-\frac{1}{2}\sigma^2\,\mathrm{Tr}\left((\nabla_x\nabla_x^T)m_0\right)=-\lambda_0 m_2+\lambda_1 m_2^z+\lambda_0\frac{q}{w}M_2$$
$$-\lambda_1\frac{q}{w}M_2^z+\mu(M_0)\int_{\mathbf{Z}}\int_{\mathbf{Z}}\mathcal{X}(x,z,z^{'})g(t,x,v,z^{'})A(x)dz^{'}dz. \tag{31}$$

With classical scaling arguments (see Engwer et al. 2015 for more details), we obtain $M_0^z=m_0^z=0$ and $m_0=\frac{q(x,v)}{w}M_0$. On account of that, using the symmetry assumption, i.e., $\mathbb{E}_q=0$, from (30), we obtain $M_1^z=0$, and

$$m_1^z=\frac{f^{'}(A(x))\langle v,\nabla_x A(x)\rangle\frac{q}{w}M_0}{\lambda_0+A(x)k^+ +k^-}.$$

Moreover, considering (29) and following the analysis in Othmer and Hillen (2000), Engwer et al. (2015), we get $M_1=0$, and

$$m_1=\frac{1}{\lambda_0}\Big[-\langle\nabla_x m_0,v\rangle+\lambda_1\Big(\frac{f^{'}(A(x))\langle v,\nabla_x A(x)\rangle\frac{q}{w}M_0}{\lambda_0+A(x)k^+ +k^-}\Big)\Big].$$

Replacing it into (31) and integrating over $\mathbf{V}$, we get:

$$\partial_t M_0+\int_{\mathbf{V}}\langle\nabla_x m_1,v\rangle dv-\frac{1}{2}\int_{\mathbf{V}}\sigma^2\,\mathrm{Tr}(\nabla_x\nabla_x^T)(m_0)dv=\mu(M_0)A(x)M_0, \tag{32}$$

where

$$\frac{1}{2}\sigma^2 \int_{\mathbf{V}} \mathrm{Tr}(\nabla_x \nabla_x^T)(m_0)dv = \frac{1}{2}\sigma^2 \int_{\mathbf{V}} \mathrm{Tr}(\nabla_x \nabla_x^T)\Big(\frac{q(x,v)}{w} M_0\Big)dv = \frac{1}{2}\sigma^2 \Delta(M_0).$$

Therefore, the evolution equation for M_0 reads

$$\partial_t M_0 - \nabla_x \cdot \big(D_T(x)\nabla_x M_0\big) + \nabla_x \cdot \big(D_T(x) l(A(x)) \nabla_x A(x) M_0 - P_T(x) M_0\big) - \frac{1}{2}\sigma^2 \Delta(M_0) = \mu(M_0) A(x) M_0,$$

where

$$l(A(x)) := \frac{\lambda_1 f'(A(x))}{\lambda_0 + A(x)k^+ + k^-}, \tag{33}$$

denotes the function that carries the information about the influence of the subcellular dynamics, while

$$D_T(x) := \frac{1}{\lambda_0} \int_{\mathbf{V}} \frac{q(x,v)}{w} v \otimes v dv, \tag{34}$$

refers to the macroscopic tumour diffusion tensor. In addition, the tumour drift velocity is given by

$$P_T(x) := \frac{1}{\lambda_0} \int_{\mathbf{V}} \nabla_x \left(\frac{q(x,v)}{w}\right) v \otimes v dv. \tag{35}$$

In view of the results obtained in Engwer et al. (2015), the ϵ-correction terms for M can be left out and, after ignoring the higher order terms and discarding subscripts, we obtain the following evolution equation characterising the macroscopic glioma density:

$$\partial_t M - \nabla_x \cdot \big(D_T(x)\nabla_x M\big) + \nabla_x \cdot \big(D_T(x) l(A(x)) \nabla_x A(x) M - P_T(x) M\big) - \frac{1}{2}\sigma^2 \Delta M = \mu(M) A(x) M. \tag{36}$$

More details about the existence, uniqueness, and non-negativity of the solution of the related parabolic problem with homogeneous Neumann boundary conditions are provided in Appendix 1

4 Numerical simulations

We perform 2D simulations of the macroscopic equation for the tumour cells (36) to study the impact of both the subcellular dynamics and the stochastic parameter σ on the overall tumour evolution.

Table 1 Model parameters

Parameter	Description	Value (unit)	Source
s	Speed of tumour cells	0.21×10^{-3} (mm s^{-1})	Chicoine and Silbergeld (1995)
λ_0	Turning frequency in $\mathcal{L}$	$[0.25, 5]$ (s^{-1})	Based on Sidani et al. (2007)
λ_1	Turning frequency in $\mathcal{L}$	$[-5, 5]$ (s^{-1})	Based on Engwer et al. (2016a)
μ_0	Tumour proliferation rate	8.44×10^{-7} (s^{-1})	Hunt (2018)
K_M	Tumour carrying capacity	$\approx 10^6$ (cells mm^{-3})	Milo et al. (2010)
σ	Free stochastic parameter	$[0.01 - 0.2]$ (mm^2 s^{-1})	Proposed range

With this aim, we first specify parameters and coefficient functions involved in the equation. Concerning the tumour diffusion tensor $D_T(x)$ in (34), we numerically compute it using the orientation distribution function given in (16), where $\mathbb{D}(x)$ represents the water diffusion tensor obtained from processing (patient-specific) DTI data. Taking advantage of this DTI information, for the macroscopic tissue density $A(x)$ we assume the following expression

$$A(x) = FA(\mathbb{D}(x)), \tag{37}$$

where FA refers to the fractional anisotropy of the tissue. We refer to Engwer et al. (2015) for its definition. This choice is motivated by the fact that the fractional anisotropy represents a measure of the fiber alignment and, since in this setting fiber alignment is guiding cell migration, it is reasonable to assume that the function $A(x)$ expresses higher values where the tissue is more anisotropic.

Following several previous works [e.g. see (Engwer et al. 2016a; Conte et al. 2020)], for the growth rate $\mu(M)$ we employ a logistic growth term defined as

$$\mu(M) = \mu_0 \left(1 - \frac{M}{K_M}\right),$$

with μ_0 the constant growth coefficient and K_M the tumour carrying capacity. Finally, we report in Table 1 the range for the constant parameter values involved in the macroscopic setting (36). The values for the stochastic parameter σ are proposed based on the ranges of the other parameters.

We present 2D numerical simulations performed with a self-developed code in Matlab (MathWorks Inc., Natick, MA). The computational domain is a horizontal brain slice reconstructed from MRI scans. The DTI dataset used to compute $D_T(x)$ was acquired at the Hospital Galdakao-Usansolo (Galdakao, Spain), and approved by its Ethics Committee: all the methods employed were in accordance to approved guidelines. A Galerkin finite element scheme for the spatial discretisation is considered, together with an implicit Euler scheme for the time discretisation. For the initial condition, we consider a Gaussian-like aggregate of tumour cells centered at $(x_0, y_0) = (-35, -41)$, situated in the left-bottom part of the brain slice. To be specific,

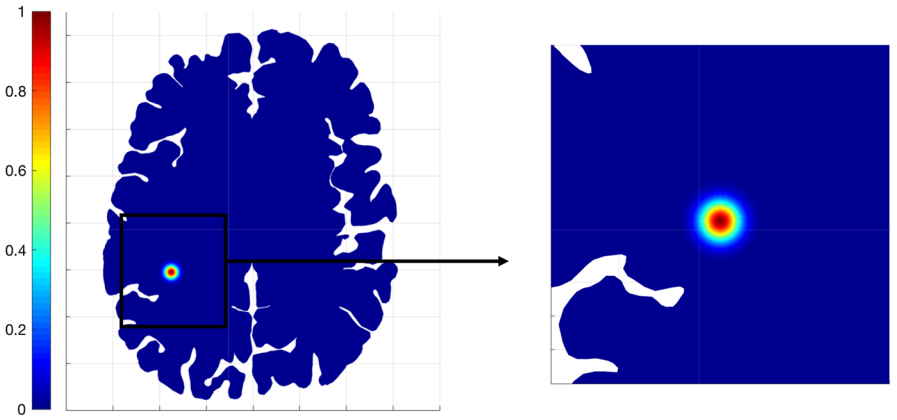

Fig. 1 Initial condition of Eq. (36)

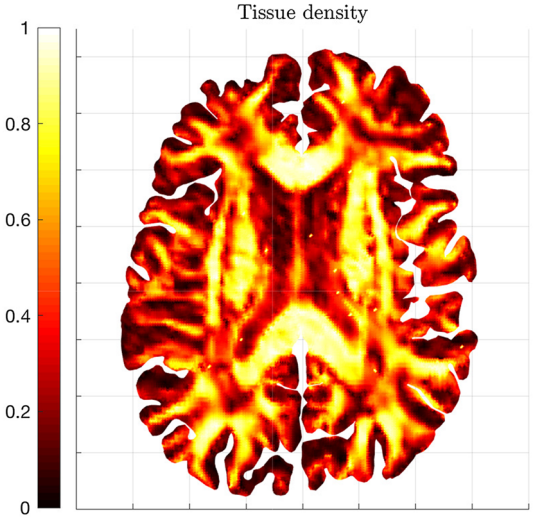

Fig. 2 Healthy tissue density

$$M_0 = e^{\frac{(x-x_0)^2+(y-y_0)^2}{8}}.$$

Figure 1 shows the initial condition on the entire 2D brain slice and in the corresponding zoomed region $\mathbf{X} = [-60, -10] \times [-65, -15]$.

Moreover, Fig. 2 shows the initial tissue density estimated with (37). In particular, yellow areas refer to regions where the fibers are highly aligned and, thus, the value of $FA(\mathbb{D}(x))$ is closer to one, while black-red areas refer to more isotropic regions, where the fibers are randomly distributed Engwer et al. (2015).

We present different sets of simulations to obtain insight into several features characterising the proposed approach. Precisely,

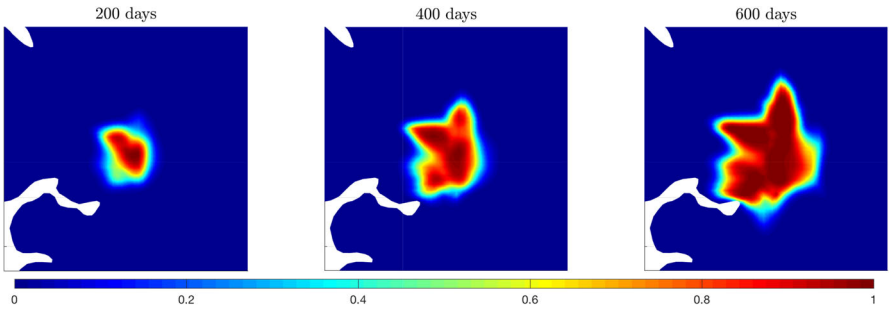

Fig. 3 System evolution. Numerical simulation of Eq. (36) with the parameters listed in Table 1 and for $\lambda_0 = \lambda_1 = 0.8\ (s^{-1})$. The tumour evolution is shown after 200, 400, and 600 days

(A) we consider the model for $\sigma = 0$ and we evaluate the effects of the variation of λ_1 and λ_0 on tumour evolution;
(B) we fix the value of λ_0 and λ_1 and we assess the effects of the variation of σ on tumour evolution, i.e., the role of the stochastic parameter in the overall dynamics;
(C) we consider different combinations of λ_1 and σ and we show how their respectively effects merge;
(D) following the approach proposed in Bogdańska et al. (2017), we discuss the effects of λ_0, λ_1, and σ on the estimation of the onsets of malignant transformation from low grade to high grade gliomas.

Starting from the numerical test **(A)**, we analyse the effects of varying λ_1 (referring to it as experiment **A.1**) and λ_0 (referring to it as experiment **A.2**). These experiments are motivated by the fact that obtaining a clear biological estimation for λ_0 and, especially, for λ_1 is quite difficult. Thus, understanding the impact of their variation becomes a fundamental point to address. As described in Sect. 3.1.2, λ_0 refers to the basal turning frequency of an individual cell, while λ_1 takes into account the role of the receptor dynamics in the evolution. Recalling the expression of the turning rate $\lambda(z)$, we could describe the constant parameters λ_0 and λ_1 as the weights of the receptors-independent and receptors-dependent cell turning, respectively. Starting from the analysis on the parameter λ_1 and in line with some studies concerning the effects of its variability (Hunt 2018) on tumour evolution, we consider the range $\lambda_1 \in [-5, 5]\ (s^{-1})$ and we assess the effects of changes in both its sign and modulus. Considering that the turning rate $\lambda(z) = \lambda_0 - \lambda_1 z$ has to be non-negative, we should ensure that $\lambda_0 \geq \lambda_1 z$, meaning that

- if $\lambda_1 \geq 0$, the non-negativity is ensured for $\lambda_0 \geq \lambda_1/2$;
- if $\lambda_1 \leq 0$, the non-negativity is ensured for $\lambda_0 \geq \lambda_1$.

Thus, to obtain reasonable values of the turning rate, we should assume $\lambda_1 \leq \lambda_0$. Although we are aware that negative values of these parameters are not sustained by biological observations, we also include them in our analysis because we want to assess the sensitivity of our results to these parameter changes. In Fig. 3, we firstly show the evolution of the tumour density over time in the limit case in which $\lambda_0 = \lambda_1 = 0.8\ (s^{-1})$.

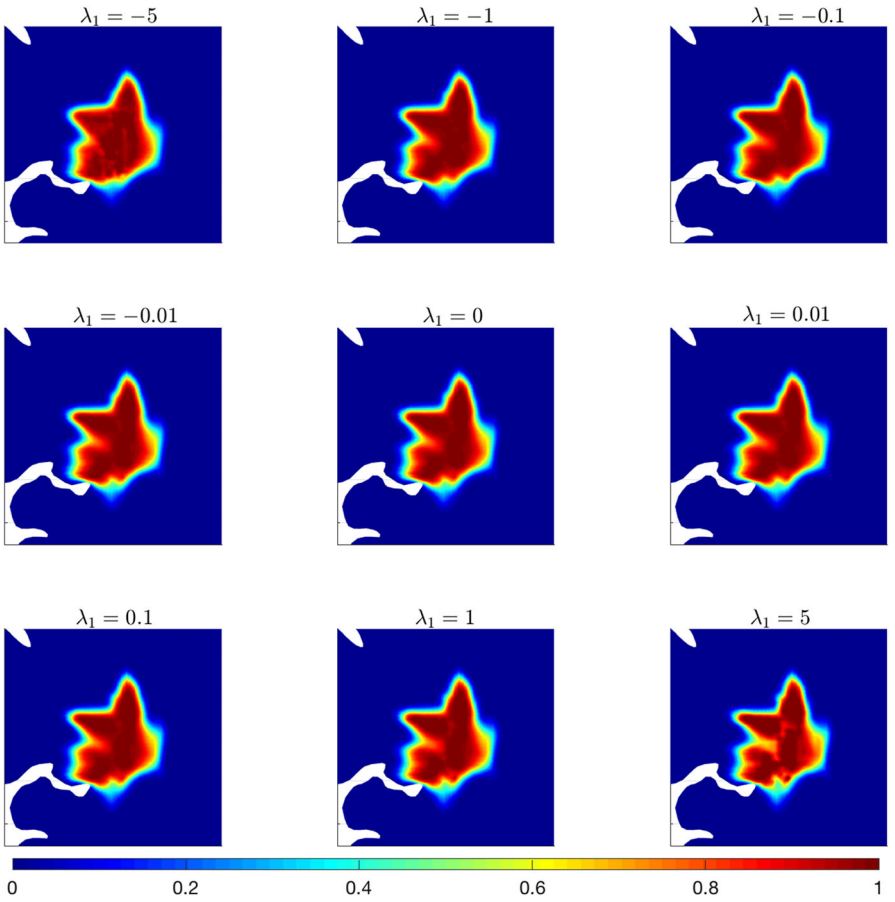

Fig. 4 Experiment (A.1). Numerical simulations of Eq. (36) with the parameters listed in Table 1, $\lambda_0 = 0.8$ (s^{-1}) and for different values of λ_1 (s^{-1}). The tumour evolution is shown after 600 days

We notice how cell spreading is highly influenced by the underlying fiber structure. Cells clearly tend to move along preferential directions, determined by the fiber bundles, and this gives rise to a heterogeneous tumour mass with an irregular shape, which is a common characteristic for this kind of brain tumours.

Referring to the tumour situation at the last time step, i.e., after 600 days, we compare the tumour evolution for different values of the parameter $\lambda_1 \in [-5, 5]$ (s^{-1}), as described in experiment **A.1**. Results are shown in Fig. 4.

The main effect of varying λ_1 consists in obtaining a greater or lower level of heterogeneity in the distribution of the tumour cells inside the tumour mass. The external border of the neoplasia, in fact, does not seem to be particularly affected, while the internal dissemination of the cells shows evident changes when λ_1 varies from large-negative values to large-positive values. In particular, clear differences with respect to the case $\lambda_1 = 0$ can be observed for quite large values of the parameter ($|\lambda_1| > 1$), while the evolution is qualitatively similar in the cases $|\lambda_1| < 1$. Such

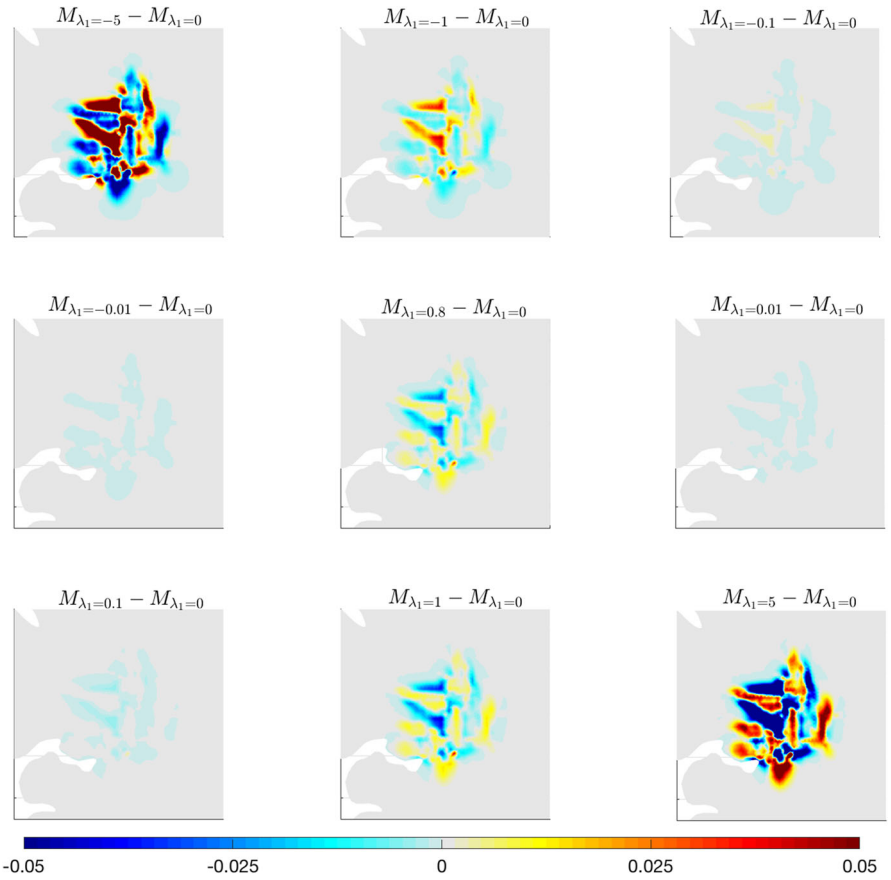

Fig. 5 Details of experiment (A.1). Differences between the solution of system (36) with $\lambda_1 = 0$ and the solution obtained for λ_1 varying in the interval $[-5, 5]$ (s^{-1}). Results are shown after 600 days. Here $\lambda_0 = 0.8\,(s^{-1})$, while the remaining parameters are taken from Table 1

differences can be better observed in Fig. 5, where the differences between the solution of system (36) for $\lambda_1 = 0\,(s^{-1})$ and the solution of the same system for the different values of λ_1 used in Fig. 4 are shown.

The impact of λ_1 variation can be immediately grasped. There is a clear difference in the spreading inside the tumour mass and in the cell response to the anisotropy of the brain tissue. The impact becomes stronger when λ_1 increases in modulus, and especially for $|\lambda_1| > 1$. In this case, in fact, the haptotactic component of the dynamics is stronger (in an attractant or repellent way, depending on the sign of λ_1) and, thus, the heterogeneity of the underlying brain tissue has a larger impact on the dynamics. The mechanism that drives cell migration along the tissue structure can be visualised in detail in Fig. 6, where the leading eigenvector of the tensor $D_T(x)$ (related to the fiber direction) is plotted together with the differences in the tumour density at 600 days for $\lambda_1 = 5\,(s^{-1})$ and $\lambda_1 = -5\,(s^{-1})$.

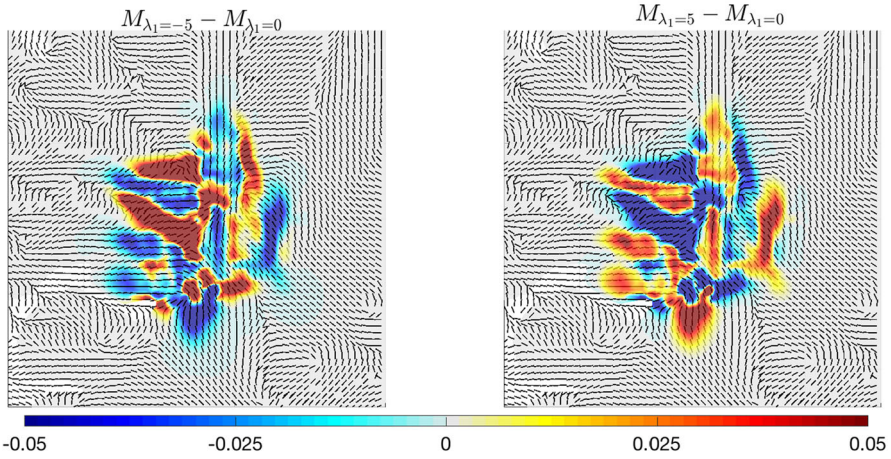

Fig. 6 Details of experiment (A.1). Differences between the solution of system (36) with $\lambda_1 = 0$ and the one obtained for $\lambda_1 = -5$ (s^{-1}) (left plot) and $\lambda_1 = 5$ (s^{-1}) (right plot) after 600 days. The differences are plotted against the fiber direction

Recalling the expression given for the tissue density (37), from the left plot of Fig. 6 we notice that, where the fibers are strongly aligned (e.g. along the central vertical bound), we obtain negative values of the difference $M_{\lambda_1=-5} - M_{\lambda_1=0}$. Here, in fact, the gradient of tissue $A(x)$ driving the haptotactic movement is bigger and, due to the negative value of λ_1, cells tend to avoid this area, moving away from it. Conversely, looking at the right plot of Fig. 6, we obtain exactly the reverse behaviour. In fact, the positive value of λ_1 leads to a much stronger haptotactic movement toward these fiber bundles. Thus, the difference shows positive values in the same regions described above.

We then test the effect of varying the parameter λ_0, as described in experiment **A.2**. Results of this test are shown in Fig. 7, where the difference between the solution of (36) for $\lambda_0 = 0.8\,(s^{-1})$ and the one obtained for λ_0 varying in the interval $[0.25, 5](s^{-1})$ are illustrated.

We observe two different trends for $\lambda_0 \geq 0.8$ or $\lambda_0 \leq 0.8$. Smaller values of the parameter lead to a larger spreading of the tumour cells with respect to the case $\lambda_0 = 0.8$, while larger values of it lead to a reduced invasion of the tumour mass. In fact, smaller values of λ_0 mean a reduced random turning of the cells, thus a greater persistence in their migration, which macroscopically translates into a large spread. Instead, larger values of λ_0 imply a larger frequency of cell turning and, thus, a macroscopic lower degree of persistence and spread in the tissue. In particular, the main difference is in the region of the outer rim of the neoplasia. This is also evident from the fact that λ_0 appears in the denominator of $\mathbb{D}_T(x)$, the macroscopic tumour diffusion tensor and, thus, smaller values of λ_0 would enhance cell diffusion.

Concerning the numerical test **(B)**, we fix $\lambda_0 = \lambda_1 = 0.8\,(s^{-1})$ and we vary the value of the parameter σ relating to the variability of the cell velocity in the microscopic model (13) and, thus, leading the additional diffusion term appearing in the

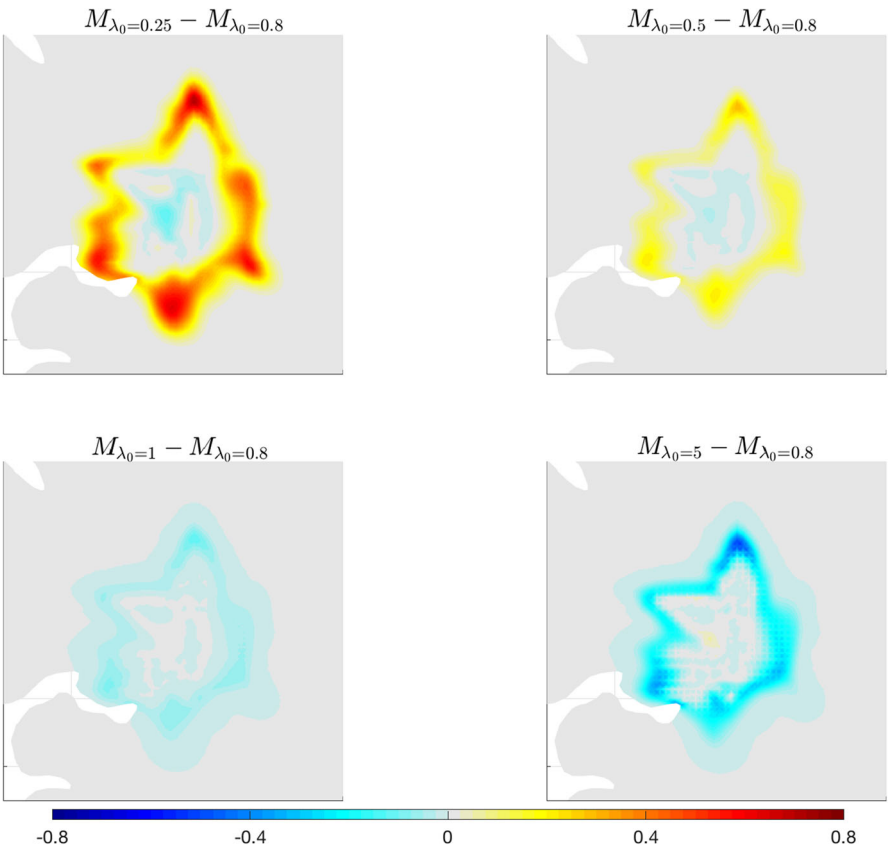

Fig. 7 Experiment (A.2). Differences between the solution of system (36) with $\lambda_0 = 0.8\ (\mathrm{s}^{-1})$ and the one obtained for λ_0 varying in the interval $[0.25, 5]\ (\mathrm{s}^{-1})$. Results are shown after 600 days. The remaining parameters are taken from Table 1, while $\lambda_1 = 0.8\ (\mathrm{s}^{-1})$

macroscopic model (36). Results of the simulations for $\sigma \in [0.01 - 0.2]\ (\mathrm{mm}^2 \cdot \mathrm{s}^{-1})$ are shown in Fig. 8.

As expected from equation (36), the effect of the parameter σ consists of a larger spread of the tumour cells inside the brain tissue. In particular, the larger the value of σ is, the stronger the diffusion phenomenon characterising glioma cells appears. For large values of σ, we observe more regular tumour borders and a more isotropic cell migration because the additional diffusion term does not depend on the diffusion tensor (34). These features can be better appreciated in Fig. 9, where the differences between the solution of equation (36) for $\sigma \neq 0$ and for $\sigma = 0$ are shown.

This figure clearly depicts an extensive and more homogeneous diffusion of the tumour mass for large values of σ. We obtain, in fact, negative values of the differences only in areas inside the tumour core (due to the balance between a faster spread and the same cell proliferation rate), while positive differences in the areas around the tumour border. In particular, comparing the first rows of Figs. 9 and 7, we notice that the increase of σ values has an effect similar to the decrease of λ_0 values, i.e., a larger

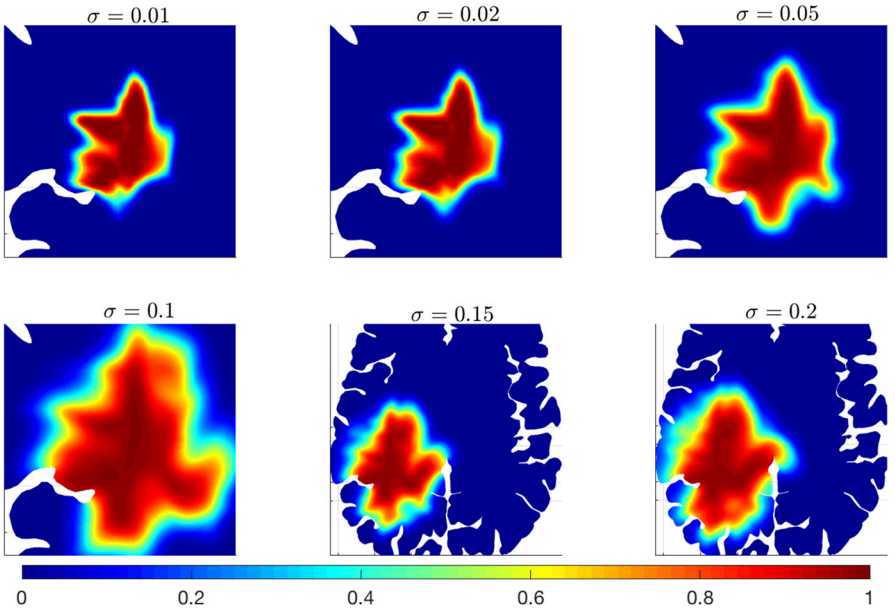

Fig. 8 Experiment (B). Numerical simulations of Eq. (36) with parameters listed in Table 1 and for different values of σ. The tumour evolution is shown after 600 days. Values of σ are expressed in $\text{mm}^2 \cdot s^{-1}$. The figures referring to the cases $\sigma = 0.15$ and $\sigma = 0.2$ are shown on a less zoomed region to better assess the tumour invasion in the tissue

tumour spread in the area of tumour outer rim. It is interesting to observe how the same macroscopic cell behaviour is obtained from two different microscopic processes. In fact, increasing σ allows for a stronger effect of the stochastic component related to the variation of cell velocity, while decreasing λ_0 reduces the random turning of the cells and determines a greater persistence in their direction of migration.

Referring to test **(C)**, we analyse the interplay between the effects of the parameters λ_1 and σ. In particular, we consider three different combinations of them:

(C.1) a high value of λ_1 and a small value of σ;
(C.2) high values of both λ_1 and σ;
(C.3) low values of both λ_1 and σ.

Results of these experiments are shown in Fig. 10.

From this figure, we notice how the respective effects of the variation of λ_1 and σ (which we separately observed in the previous experiments **(A.1)** and **(B)** merge. In fact, in the scenario **(C.1)** (first row of Fig. 10), the spread of the tumour cells is relatively confined due to the small value of σ. This spread follows the main fiber bundles present in the interested region, as λ_1 is large and drives the cell turning response to the fiber network. Moreover, the inner region of the tumour mass shows a high level of heterogeneity, as additional effect of the high value of λ_1. This heterogeneity becomes particularly evident comparing the tumour evolution at 600 days in the scenarios **(C.1)** and **(C.3)** (top and bottom row of Fig. 10), which use the same values of σ, but different values of λ_1. Considering the combination of high values for both parameters

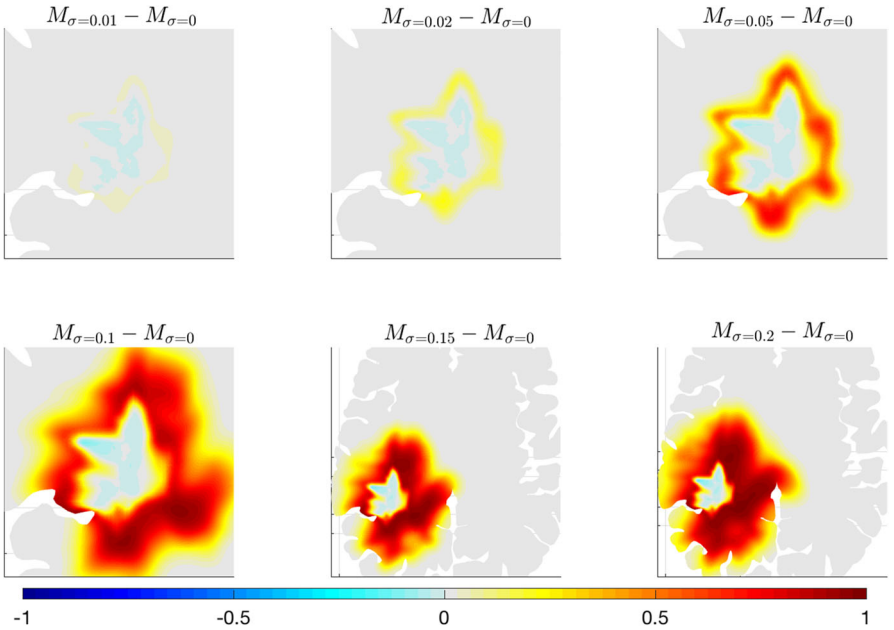

Fig. 9 Details of experiment (B). Differences between the solution of system (36) for $\sigma = 0$ and the one obtained for $\sigma \in [0.01, 0.2]$ (mm^2 s^{-1}). Results are shown after 600 days. The remaining parameters are taken from Table 1. The figures referring to the cases $\sigma = 0.15$ and $\sigma = 0.2$ are shown on a less zoomed region to better observe the tumour invasion in the tissue

Table 2 Estimations of the onsets of malignant transformation τ_{OSM} for different values of λ_1, σ, and λ_0

λ_1 (s^{-1})	-5	-1	-0.1	-0.01	0	0.01	0.1	0.8	1	5
τ_{OSM} (days)	299	316	321	321	321	321	321	321	322	327
σ (mm^2 s^{-1})	0.01	0.02	0.05	0.1	0.15	0.2				
τ_{OSM} (days)	321	334	365	492	552	564				
λ_0 (s^{-1})	0.25	0.5	0.8	1	5					
τ_{OSM} (days)	400	341	321	305	285					

(scenario **(C.2)**) leads to a larger spread of the tumour mass, as effect of the additional diffusion term driven by σ, and a different internal arrangement of the tumour cells compared with the bottom-left plot of Fig. 8 (where the tumour evolution is shown at $T = 600$ days for $\sigma = 0.1$ (mm$^2 \cdot$ s^{-1}) and $\lambda_1 = 0.8$ (s^{-1}). This is still an effect of the higher value of λ_1, here set at $\lambda_1 = 5$ (s^{-1}). Finally, the combination of low values for both σ and λ_1 used for scenario **(C.3)** determines a smoothness of the internal distribution of tumour cells as well as a reduced cell spread in the healthy tissue.

For the last test **(D)**, we discuss the onsets of malignant transformation from low grade glioma (LGG) to high grade glioma (HGG) in relation to the possible variations of the parameters λ_0, λ_1, and σ. LGGs are usually slowly-growing, infiltrative tumour with a very unpredictable clinical course. Most LGG patients face transformation of

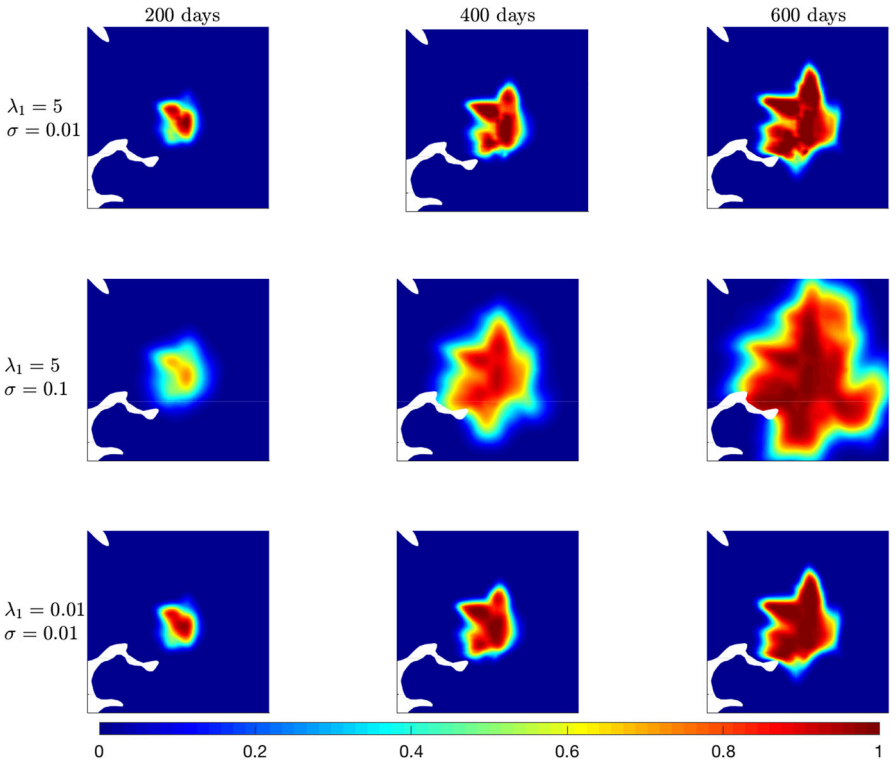

Fig. 10 Experiment (C). Numerical simulations of Eq. (36) with different combinations of λ_1 and σ. Columns refer to the three different time instants 200, 400, and 600 days, respectively. Rows refer to scenarios **(C.1)**, **(C.2)**, and **(C.3)**, respectively. The remaining parameters are listed in Table 1. Values of λ_1 and σ are expressed in s^{-1} and $mm^2 \cdot s^{-1}$, respectively

their tumour into higher grade one, with a worse prognosis. This process is known as malignant transformation and it is usually defined on the basis of contrast enhancement on MRI scans or histopathological evidence. In line with the approach proposed in Bogdańska et al. (2017), we estimate the time instant τ_{OSM} of the onset to the malignant transformation of cells into a more aggressive high grade tumour. The main aim of the proposed experiment **(D)** consists in showing how our approach is able to replicate the same qualitative behaviours of Bogdańska et al. (2017) (where a comparison with patient data is proposed), but with a more detailed and precise description of the microscopic processes related to cell migration. Specifically, τ_{OSM} is defined as the first time instant at which the LGG cell density becomes greater than a certain threshold M_{crit}, which we set to $0.6K_M$ Bogdańska et al. (2017). We run several numerical tests varying one parameter at the time and estimating the resulting time of onset of the malignancy. Table 2 collects the results of these experiments.

We observe that the parameter λ_1 seems to not have such an evident impact on the time of onset of malignancy. In fact, τ_{OSM} varies only of ± 28 days. Instead, both λ_0 and σ strongly affect the estimation of τ_{OSM}. In Fig. 11 the estimated values of τ_{OSM} with respect to λ_0 and σ are plotted together with the corresponding interpolant curves,

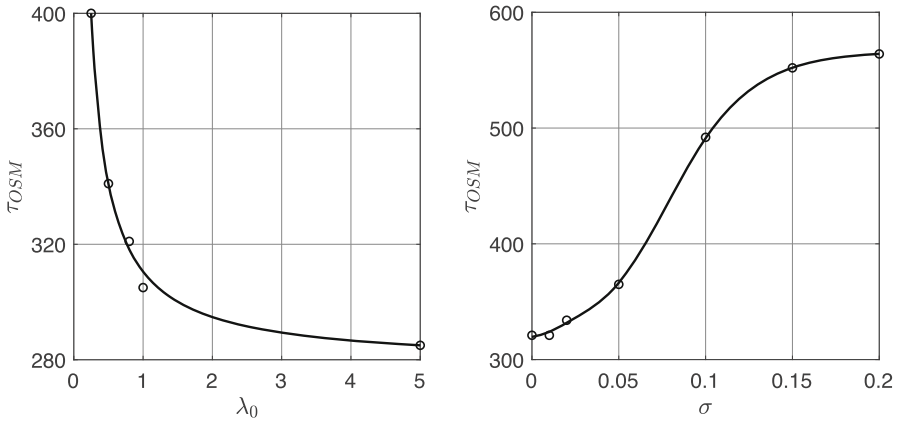

Fig. 11 Experiment (D). Estimation of the time of onset of malignant transformation τ_{OSM} for different values of the turning rate λ_0 and the free parameter σ. The remaining parameters are taken as in Fig. 3

showing the trends of $\tau_{OSM} = \tau_{OSM}(\lambda_0)$ (left plot of Fig. 11) and $\tau_{OSM} = \tau_{OSM}(\sigma)$ (right plot of Fig. 11).

Increasing the value of λ_0 leads to a reduction of the time τ_{OSM} at which LGG turns into HGG, while increasing σ has the reverse effect, i.e., it leads to an increase of τ_{OSM}. The parameter λ_0 is, in fact, related to the tumour responsiveness to the tissue structure, and smaller values of this parameter refer to a loss of responsiveness, which is a common characteristic in HGG. Moreover, observing that the overall diffusion coefficient of tumour cells in equation (36) is proportional to $\frac{1}{\lambda_0} + \frac{\sigma^2}{2}$, increasing σ (or equivalently decreasing λ_0) corresponds to an increase of this diffusion coefficient. Thus, comparing these results with the ones shown in Bogdańska et al. (2017) (e.g. see Figure 7 in there), we notice a good qualitative agreement between them and a similar behaviour for the evolution τ_{OSM}. We would like to remark that this is only a first possible approximation for the estimation of τ_{OSM} and we are aware that there are several other factors involved in the definition of the transformation from LGG to HGG, apart from the increase in the tumour density. Surely, the tumour density values have an evident impact on the definition of τ_{OSM}, however, from a mathematical point of view, it is difficult to provide a formal definition for it. Thus, as a first attempt, we decide to rely on the definition given in Bogdańska et al. (2017) for τ_{OSM}, leaving its possible extensions for future works.

5 Discussion

To the best of our knowledge, this is the first hierarchical stochastic model in which piecewise diffusion Markov processes are used to describe glioma cell motion within a multiscale framework. We start with the description of glioma cell movement at the microscopic scale using a PDifMP, which combines a stochastic model for cell motility and a deterministic one for cell migration. The latter looks at the response of glioma cells to external environmental cues. The extended generator of the formulated

PDifMP takes the form of an integro-differential equation in all the involved variables. Its solution yields the density of the transition probability of the Markov process. Using scaling arguments, we then obtain the equation describing the evolution of the tumour density at the macroscopic level. In this way, our approach allows us to take into account the macroscopic level properties as well as the features characterising the microscopic processes.

Using numerical simulations of the macroscopic setting we analyse the role and influence of both the parameters involved in the jump rate function λ of the PDifMP and the parameter σ related to the stochastic variability in the cell velocity. In particular, we observe how the parameter λ_0 at the microscopic scale promotes a major spreading of the tumour mass inside the brain tissue, regardless of the specific brain structure, while λ_1 relates to cell responsiveness to the guided movement along the brain fibers. The fully detailed formulation of glioma cell motion with the PDifMP allows us to observe that the jump rate function determines the distribution of the waiting times of the process being in a particular state. Thus, for a constant jump rate ($\lambda = \lambda_0$) there is no influence of the microenvironment on the motion and a larger frequency of cell turning determines at the macroscopic scale a reduced migration along the fibers. Instead, including the term $\lambda_1 z$ results in an increase in reorientations in response to the brain structure and, thus a visible heterogeneity inside the tumour bulk. A particularly interesting result is obtained by comparing the numerical experiments **A.2** and **B**. In fact, we show how a similar macroscopic behaviour—large cell spreading around the outer rim of the tumour -can result from two different sources at the microscopic level: either from increasing the value of σ and thus the diffusion of cells, or from reducing the value of λ_0 and thus the random cell rotations, resulting in higher cell persistence.

A further aspect of novelty, which distinguishes our approach from well-known multiscale models of this type (Engwer et al. 2015, 2016a, b), is the inclusion of an analysis of the transition to malignancy of the tumour mass. In particular, by accepting the hypothesis that the loss of responsiveness of glioma cells to the tissue structure can be seen as a sign of the transition from LGG to HGG, we numerically show that the time at which this transition happens can be estimated with our approach. Moreover, we highlight how it is influenced by the parameters σ and λ_0, looking at the related biological processes that may explain it. The obtained results are perfectly in line with the ones presented in Bogdańska et al. (2017), confirming the reliability of the proposed approach.

With our work, we aim at emphasising how the use of PDMP or PDifMP for the description of the phenomena leading cell movement is of paramount importance for rigorously modelling the cellular scale processes. An interesting point would concern a numerical comparison of the cell behaviours at the different scales (microscopic and macroscopic) with either the deterministic or the stochastic formulation. Moreover, in the present notes, glioma cell motion is described in relation to the binding with the tissue, but the proposed approach can be extended in order to incorporate other biologically relevant aspects of tumour progression. For instance, following (Conte and Surulescu 2021; Conte et al. 2022), the influence of microenvironmental acidosis on glioma cell migration and the consequent pH-repellent chemotactic process can be considered. This could be done assuming different expressions for the jump rate function of the PDifMP, e.g. allowing its dependence on different interactions between

cells and microenvironment or relating it to the tumour response to treatments. Additionally, following the approach recently proposed in Darrigade et al. (2022), we could also model proliferation at the microscale using PDMPs, among many other biological aspects, and see their influence on the macroscopic density.

Another interesting direction for future development concerns the modification of the jump process using stochastic differential equations to model not only jumps in the cell velocity, but also jumps in the position, trying to recover the typical feature of tumour recurrence in different (and quite far from the original tumour location) regions of the brain. Finally, here we propose a first possible way to analyse the transition to malignancy. However, as stated in the above section, this process is much more complex and we are working towards the development of an interdisciplinary study in which an extension of our approach could be used to shed light on the intricate biological processes underlying this transition.

Acknowledgements E.B. and and A.M. were supported by the Austrian Science Fund (FWF): W1214-N15, project DK14, as well as by the strategic program "Innovatives OÖ 2010 plus" by the Upper Austrian Government. M.C. acknowledges funding by the Ministry of Education, Universities, and Research through the MIUR grant Dipartimento di Eccellenza 2018-2022, Project No. E11G18000350001, and the Scientific Research Programmes of Relevant National Interest project n. 2017KL4EF3. M.C. also acknowledges the support of the National Group of Mathematical Physics (GNFM-INdAM). The authors thank Dr. Philip-Rudolf Rauch from the University Hospital for Neurosurgery, Kepler University Hospital and Prof. Luca Gerardo-Giorda from Johannes Kepler University, for many fruitful discussions and insights into the topics of low grade gliomas and mathematical modelling.

Funding Open access funding provided by Austrian Science Fund (FWF).

Declarations

Conflict of interest The authors have no competing interests to declare that are relevant to the content of this article.

Appendix A

A.1 Well-posedness of the macroscopic problem

Using the theory of monotone operators for nonlinear parabolic equations and following the approach in (Showalter 2013; Ruzicka 2004), it is possible to prove the existence, uniqueness, and non-negativity of the solution of the following parabolic

problem with homogeneous Neumann boundary conditions.

$$\begin{cases} \partial_t M - \nabla_x \cdot \left(\left(D_T(x) + \frac{1}{2}\sigma^2 \right) \nabla_x M \right. \\ \left. + \gamma(D_T(x), A(x))M \right) - \Gamma(M, A(x)) = 0, & in \quad [0,T] \times \mathbf{\Omega}, \\ \nabla_x M \cdot \hat{n} = 0 & on \quad [0,T] \times \partial\mathbf{\Omega}, \\ M(0,x) = \tilde{M}_0(x), & in \quad \mathbf{\Omega}, \end{cases} \tag{A1}$$

where

$$\gamma(D_T(x), A(x)) := P_T(x) - D_T(x) l(A(x)) \nabla_x A(x),$$

$$\Gamma(M, A(x)) := \mu(x, M) A(x) M.$$

A.1.1 Assumptions

Let $\mathbf{\Omega} \subset \mathbb{R}^3$ be a Lipschitz domain with a continuous boundary $\partial\mathbf{\Omega} \in C^{0,1}$ and let $\hat{n}$ be the normal vector to the boundary. Let $T > 0$ such that $I = [0, T]$ denotes a finite time interval. Let us define the Gelfand triple $(\mathcal{V}, \mathcal{H}, \mathcal{V}^*)$ (see Gilbarg and Trudinger 2015 for the definition) such that $\mathcal{V} = H_0^1(\mathbf{\Omega}) = W_0^{1,2}(\mathbf{\Omega})$, $\mathcal{H} = L^2(\mathbf{\Omega})$, $\mathcal{X} = L^2(I; \mathcal{V})$, and $\mathcal{V}^*$ is the dual space of $\mathcal{V}$. We also define the functional space

$$\mathcal{W} := \{M \in \mathcal{X} = L^2(I; \mathcal{V}) : \partial_t M \in L^2(I; \mathcal{V}^*)\}$$

such that $\mathcal{W} \hookrightarrow \mathcal{X}$ (using conclusion 3.98 in Ruzicka (2004) it is possible to prove the embedding).

We make the following assumptions.

A.1 The diffusion tensor $D_T(x)$ is positive definite, it belongs to the Sobolev space $W^{1,\infty}(\mathbf{\Omega})$ and its smallest eigenvalue is larger than a strictly positive constant α. Note that $D_T(x) + \frac{1}{2}\sigma^2$ is also an element of $W^{1,\infty}(\mathbf{\Omega})$.

A.2 The function $\Gamma : \mathbb{R} \mapsto \mathbb{R}$ is continuous and it satisfies

1. the growth condition

$$|\Gamma(s)| \leq c\left(1 + |s|^{r-1}\right),$$

where c is a constant, independent from space and time, and $1 \leq r < \infty$;

2. the coercivity condition

$$\inf_{s \in \mathbb{R}_+} \Gamma(s)s > -\infty.$$

A.3 The function $A(x)$ belongs to the Sobolev space $W^{1,\infty}(\mathbf{\Omega})$.

A.4 The velocity field $P_T(x)$ belongs to the Sobolev space $W^{1,\infty}(\mathbf{\Omega})$.

A.5 The term $\gamma(D_T(x), A(x))$ belongs to the Lebesgue space L^∞.

A.1.2 Existence

Theorem 2 *Let $\tilde{M}_0 \in \mathcal{H}$ and the continuous function $\Gamma : \mathbb{R} \mapsto \mathbb{R}$ satisfies the condition A.2, with $1 \leq r \leq p\frac{2+n}{n} = \frac{10}{3}$, where n denotes the spatial dimension ($n = 3$) and p refers to the p-th power of the Lebesgue space $L^p(\mathbf{\Omega})$ ($p = 2$). Then, there exists a weak solution $M \in \mathcal{W}$, such that for all $\psi \in C_0^\infty([0,T] \times \mathbf{\Omega})$ it holds that*

$$\int_0^T \langle \partial_t M, \psi \rangle_{\mathcal{V}} dt + \int_0^T \int_{\mathbf{\Omega}} ((D_T + \frac{1}{2}\sigma^2)\nabla M - \gamma(D_T, A)M)\nabla\psi dx dt$$
$$+ \int_0^T \int_{\mathbf{\Omega}} \Gamma(M)\psi(t) dx dt = 0.$$

Proof The proof is straightforward if we extend the proof proposed in Engwer et al. (2016a) to the case of the additional diffusion coefficient $\frac{1}{2}\sigma^2$. □

A.1.3 Uniqueness

Proposition 3 *Assuming that the function $\Gamma(M)$ is strictly monotone, the above solution to the macroscopic problem is unique.*

Proof See Lemma 3.38 and Theorem 3.66 in Ruzicka (2004), to prove the result. □

A.1.4 Non-negativity

Proposition 4 *The solution of the macroscopic problem with $\tilde{M}_0 \geq 0$ is non-negative.*

Proof We employ the truncation method to prove the non-negativity of the solution. Let $H(M)$ be a $C^{1,1}$ cutoff function such that:

$$\begin{cases} H(M(t,x)) = \frac{1}{2}M^2 & M \in (-\infty, 0), \\ H(M(t,x)) = 0 & M \in [0, \infty). \end{cases}$$

We denote by $\phi(t) = \int_{\mathbf{\Omega}} H(M(\bar{t}, x))dx$. We have:

$$\begin{aligned} \frac{d}{dt}\int_{\mathbf{\Omega}} H(\bar{M}(t,x))dx &= \int_{\mathbf{\Omega}} H^{'}(M)\partial_t \bar{M}(t,x)dx \\ &= \int_{\mathbf{\Omega}} H^{'}(\bar{M}\Big(\nabla_x \cdot \big((D_T + \frac{1}{2}\sigma^2)\nabla_x \bar{M}\big) - \nabla_x \cdot \big(\gamma(D_T, A)\bar{M}\big) \\ &\quad - \beta\bar{M} + \Gamma(\bar{M}, A)\Big) \\ &= \int_{\mathbf{\Omega}} M\Big(\nabla_x \cdot \big((D_T + \frac{1}{2}\sigma^2)\nabla_x \bar{M}\big) - \nabla_x \cdot \big(\gamma(D_T, A)\bar{M}\big) \\ &\quad - \beta\bar{M} + \Gamma(\bar{M}, A)\Big). \end{aligned}$$

We will now use the integration by part formula (1.69 in Yagi 2009 subsection 11.1) to get:

$$\int_{\Omega} \bar{M}\nabla_x \cdot \big((D_T + \frac{1}{2}\sigma^2)\nabla_x \bar{M}\big) = -\int_{\Omega} \nabla_x \bar{M}\big((D_T + \frac{1}{2}\sigma^2)\nabla_x \bar{M}\big)dx$$

$$\nabla_x \cdot \int_{\Omega} \big(\gamma(D_T, A)\bar{M}\big)dx = -\int_{\Omega} \nabla_x \bar{M}\big(\gamma(D_T, A)\bar{M}\big)dx.$$

Hence,

$$\begin{aligned}
&\frac{d}{dt}\int_{\Omega} H(\bar{M}(t,x))dx = -\int_{\Omega} \nabla_x \bar{M}\big((D_T + \frac{1}{2}\sigma^2)\nabla_x \bar{M}\big)dx + \int_{\Omega} \nabla_x \bar{M}\big(\gamma \bar{M}\big)dx \\
&- \beta\int_{\Omega} \bar{M}^2 dx + \int_{\Omega} \bar{M}\Gamma(\bar{M}, A)dx \\
&\leq \int_{\Omega} \nabla_x M\big(\gamma \bar{M}\big)dx + \beta\int_{\Omega} \bar{M}^2 dx + \int_{\Omega} M\Gamma(\bar{M}, A)dx \\
&\leq \int_{\Omega} |\nabla_x \bar{M}||\gamma||\bar{M}|dx + \beta\int_{\Omega} \bar{M}^2 dx + \int_{\Omega} |M||\Gamma(\bar{M}, A)|dx \\
&\leq \int_{\Omega} |\bar{M}|\gamma||\bar{M}|dx + \beta\int_{\Omega} \bar{M}^2 dx + \int_{\Omega} |\bar{M}|c(1 + |\bar{M}|^{r-1})dx \\
&\leq \int_{\Omega} |\nabla_x \bar{M}|dx \int_{\Omega} |\gamma|dx \int_{\Omega} |\bar{M}|dx + 2\beta\int_{\Omega} H(M)dx + \int_{\Omega} |\bar{M}|c(1 + |\bar{M}|^{r-1})dx, \\
&\leq \int_{\Omega} |\nabla_x M|^2 dx \int_{\Omega} |\gamma|dx \int_{\Omega} |\bar{M}|^2 dx + 2\beta\int_{\Omega} H(\bar{M})dx + \int_{\Omega} |\bar{M}|^2 c(1 + |\bar{M}|^{r-1})dx, \\
&\leq \Big(\|\nabla \bar{M}\|_{L^2}^2 \|\gamma\|_{L^\infty} + 2\beta + C_1\|\bar{M}\|_{L^r}^r\Big)\int_{\Omega} H(\bar{M})dx.
\end{aligned}$$

This implies that

$$\frac{d}{dt}H(\bar{M}) \leq C_L H(\bar{M}),$$

Consequently, using Gronwall's inequality we have

$$H(\bar{M}) \leq e^{C_L t} H(0).$$

Therefore, $\phi(0) = 0$ implies that $\phi(t) = 0$ for every $t > 0$, namely, $\bar{M}(t) \geq 0$. □

References

Adler J (1966) Chemotaxis in bacteria: motile *Escherichia coli* migrate in bands that are influenced by oxygen and organic nutrients. Science 153(3737):708–716

Aganj I, Lenglet C, Jahanshad N, Yacoub E, Harel N, Thompson PM, Sapiro G (2011) A hough transform global probabilistic approach to multiple-subject diffusion MRI tractography. Med Image Anal 15(4):414–425

Ahir BK, Engelhard HH, Lakka SS (2020) Tumor development and angiogenesis in adult brain tumor: Glioblastoma. Mol Neurobiol 57(5):2461–2478
Aubert M, Badoual M, Fereol S, Christov C, Grammaticos B (2006) A cellular automaton model for the migration of glioma cells. Phys Biol 3(2):93
Audoin M, Soegaard MT, Jauffred L (2022) Tumor spheroids accelerate persistently invading cancer cells. bioRxiv
Bect J (2007) Processus de Markov diffusifs par morceaux: outils analytiques et numériques. Ph.D. thesis, Université Paris Sud-Paris XI
Bellomo N, Bellouquid A, Nieto J, Soler J (2012) On the asymptotic theory from microscopic to macroscopic growing tissue models: an overview with perspectives. Math Models Methods Appl Sci 22(01):1130001
Bhattacharya P, Li Q, Lacroix D, Kadirkamanathan V, Viceconti M (2021) A systematic approach to the scale separation problem in the development of multiscale models. PLoS ONE 16(5):e0251297
Bielecki TR, Frankiewicz E (2006) In: Stochastic processes, optimization, and control theory: applications in financial engineering, queueing networks, and manufacturing systems. Springer, pp 35–54
Blom H (1988) In: Proceedings of the 27th IEEE conference on decision and control. IEEE, pp 1978–1983
Blom HA, Ma H, Bakker GB (2018) Interacting particle system-based estimation of reach probability for a generalized stochastic hybrid system. IFAC PapersOnLine 51(16):79–84
Bogdańska MU, Bodnar M, Piotrowska MJ, Murek M, Schucht P, Beck J, Martínez-González A, Pérez-García VM (2017) A mathematical model describes the malignant transformation of low grade gliomas: prognostic implications. PLoS ONE 12(8):e0179999
Bujorianu ML, Lygeros J (2004) In: 2004 43rd IEEE conference on decision and control (CDC) (IEEE Cat. No. 04CH37601), vol 2. IEEE, pp 1872–1877
Bujorianu ML, Lygeros J (2005) Toward a general theory of stochastic hybrid systems. HYBRIDGE Final Project Report p 9
Bujorianu ML, Lygeros J (2006) In: Stochastic hybrid systems. Springer, pp 3–30
Chicoine MR, Silbergeld DL (1995) Assessment of brain tumor cell motility in vivo and in vitro. J Neurosurg 82(4):615–622. https://doi.org/10.3171/jns.1995.82.4.0615
Clatz O, Sermesant M, Bondiau PY, Delingette H, Warfield SK, Malandain G, Ayache N (2005) Realistic simulation of the 3-d growth of brain tumors in MR images coupling diffusion with biomechanical deformation. IEEE Trans Med Imaging 24(10):1334–1346
Cloez B, Dessalles R, Genadot A, Malrieu F, Marguet A, Yvinec R (2017) Probabilistic and piecewise deterministic models in biology. ESAIM Proc Surv 60:225–245
Conte M (2021) Mathematical models for glioma growh and migration inside the brain. Ph.D. thesis, Euskal Herriko Unibertsitatea/Universidad del País Vasco
Conte M, Surulescu C (2021) Mathematical modeling of glioma invasion: acid-and vasculature mediated go-or-grow dichotomy and the influence of tissue anisotropy. Appl Math Comput 407:126305
Conte M, Gerardo-Giorda L, Groppi M (2020) Glioma invasion and its interplay with nervous tissue and therapy: a multiscale model. J Theor Biol 486:110088
Conte M, Dzierma Y, Knobe S, Surulescu C (2022) Mathematical modeling of glioma invasion and therapy approaches. arXiv preprint arXiv:2203.11578
Crudu A, Debussche A, Muller A, Radulescu O (2012) Convergence of stochastic gene networks to hybrid piecewise deterministic processes. Ann Appl Probab 22(5):1822–1859
Darrigade L, Haghebaert M, Cherbuy C, Labarthe S, Laroche B (2022) A PDMP model of the epithelial cell turn-over in the intestinal crypt including microbiota-derived regulations. J Math Biol 84(7):1–67
Davis MH (1984) Piecewise-deterministic Markov processes: a general class of non-diffusion stochastic models. J R Stat Soc Ser B (Methodol) 46(3):353–376
Demuth T, Berens ME (2004) Molecular mechanisms of glioma cell migration and invasion. J Neuro-oncol 70(2):217–228
Düchting W, Dehl G (1980) Spread of cancer cells in tissues: modelling and simulation. Int J Bio-med Comput 11(3):175–195
Düchting W, Vogelsaenger T (1981) Three-dimensional pattern generation applied to spheroidal tumor growth in a nutrient medium. Int J Bio-Med Comput 12(5):377–392
Düchting W, Vogelsaenger T (1985) Recent progress in modelling and simulation of three-dimensional tumor growth and treatment. Biosystems 18(1):79–91
Dunn G, Brown A (1987) A unified approach to analysing cell motility. J Cell Sci 1987(Supplement-8):81–102

Ellis RS (1973) Chapman–Enskog–Hilbert expansion for a Markovian model of the Boltzmann equation. Commun Pure Appl Math 26(3):327–359
Engwer C, Hillen T, Knappitsch M, Surulescu C (2015) Glioma follow white matter tracts: a multiscale DTI-based model. J Math Biol 71(3):551–582
Engwer C, Hunt A, Surulescu C (2016a) Effective equations for anisotropic glioma spread with proliferation: a multiscale approach and comparisons with previous settings. Math Med Biol J IMA 33(4):435–459
Engwer C, Knappitsch M, Surulescu C (2016b) A multiscale model for glioma spread including cell-tissue interactions and proliferation. Math Biosci Eng 13(2):443
Fontbona J, Guerin H, Malrieu F (2010) Quantitative estimates for the long time behavior of a PDMP describing the movement of bacteria. ArXiv e-prints
Frantz C, Stewart KM, Weaver VM (2010) The extracellular matrix at a glance. J Cell Sci 123(24):4195–4200
Gabbiani F, Cox SJ (2017) Mathematics for neuroscientists. Academic Press
Gao X, McDonald JT, Hlatky L, Enderling H (2013) Acute and fractionated irradiation differentially modulate glioma stem cell division kinetics. Cancer Res 73(5):1481–1490
Gardiner CW (1985) Handbook of stochastic methods: for physics, chemistry and the natural sciences. Springer, Berlin
Genadot A, Thieullen M (2014) Multiscale piecewise deterministic Markov process in infinite dimension: central limit theorem and Langevin approximation. ESAIM Probab Stat 18:541–569
Giese A, Westphal M (1996) Glioma invasion in the central nervous system. Neurosurgery 39(2):235–252
Giese A, Kluwe L, Laube B, Meissner H, Berens ME, Westphal M (1996) Migration of human glioma cells on myelin. Neurosurgery 38(4):755–764
Gilbarg D, Trudinger NS (2015) Elliptic partial differential equations of second order, vol 224. Springer
Giovanna M, Kaye AH (2007) Integrins: molecular determinants of glioma invasion. J Clin Neurosci 14(11):1041–1048
Glioma Description. https://www.aans.org/en/Patients/Neurosurgical-Conditions-and-Treatments/Brain-Tumors#:~:text=Gliomas
Harpold HL, Alvord EC Jr, Swanson KR (2007) The evolution of mathematical modeling of glioma proliferation and invasion. J Neuropathol Exp Neurol 66(1):1–9
Hatzikirou H, Basanta D, Simon M, Schaller K, Deutsch A (2012) 'go or grow': the key to the emergence of invasion in tumour progression? Math Med Biol J IMA 29(1):49–65
Hillen T (2004) On the l^2-moment closure of transport equations: the cattaneo approximation. Discrete Contin Dyn Syst B 4(4):961
Hillen T (2005) On the l^2-moment closure of transport equations: the general case. Discrete Contin Dyn Syst B 5(2):299
Hillen T (2006) M5 mesoscopic and macroscopic models for mesenchymal motion. J Math Biol 53(4):585–616
Hillen T, Painter KJ (2013) In: Dispersal, individual movement and spatial ecology. Springer, pp 177–222
Hunt A (2018) DTI-based multiscale models for glioma invasion. Ph.D. thesis, Technische Universität Kaiserslautern
Jbabdi S, Mandonnet E, Duffau H, Capelle L, Swanson KR, Pélégrini-Issac M, Guillevin R, Benali H (2005) Simulation of anisotropic growth of low-grade gliomas using diffusion tensor imaging. Magn Reson Med Off J Int Soc Magn Reson Med 54(3):616–624
Kelkel J, Surulescu C (2012) A multiscale approach to cell migration in tissue networks. Math Models Methods Appl Sci 22(03):1150017
Konukoglu E, Clatz O, Bondiau PY, Delingette H, Ayache N (2010) Extrapolating glioma invasion margin in brain magnetic resonance images: suggesting new irradiation margins. Med Image Anal 14(2):111–125
Kuehn C (2016) In: Schöll E, Klapp S, Hövel P (ed.) Control of self-organizing nonlinear systems. Springer, Switzerland, Understanding Complex Systems (UCS), pp 253–271
Lorenz T, Surulescu C (2014) On a class of multiscale cancer cell migration models: well-posedness in less regular function spaces. Math Models Methods Appl Sci 24(12):2383–2436
Loy N, Preziosi L (2020) Kinetic models with non-local sensing determining cell polarization and speed according to independent cues. J Math Biol 80(1):373–421
Luzhansky ID, Schwartz AD, Cohen JD, MacMunn JP, Barney LE, Jansen LE, Peyton SR (2018) Anomalously diffusing and persistently migrating cells in 2d and 3d culture environments. APL Bioeng 2(2):026112

Metzcar J, Wang Y, Heiland R, Macklin P (2019) A review of cell-based computational modeling in cancer biology. JCO Clin Cancer Inform 2:1–13
Migration vs Motility. https://phiab.com/applications/cell-motility-and-migration
Milo R, Jorgensen P, Moran U, Weber G, Springer M (2010) BioNumbers—the database of key numbers in molecular and cell biology. Nucleic Acids Res 38(suppl_1):108941
Mosayebi P, Cobzas D, Murtha A, Jagersand M (2012) Tumor invasion margin on the Riemannian space of brain fibers. Med Image Anal 16(2):361–373
Nankep N, et al (2018) Modélisation stochastique de systemes biologiques multi-échelles et inhomogenes en espace. Ph.D. thesis, Rennes, École normale supérieure
Oksendal B (2013) Stochastic differential equations: an introduction with applications. Springer
Othmer HG, Hillen T (2000) The diffusion limit of transport equations derived from velocity-jump processes. SIAM J Appl Math 61(3):751–775
Othmer HG, Hillen T (2002) The diffusion limit of transport equations ii: Chemotaxis equations. SIAM J Appl Math 62(4):1222–1250
Painter KJ, Hillen T (2002) Volume-filling and quorum-sensing in models for chemosensitive movement. Can Appl Math Q 10(4):501–543
Painter K, Hillen T (2013) Mathematical modelling of glioma growth: the use of diffusion tensor imaging (DTI) data to predict the anisotropic pathways of cancer invasion. J Theor Biol 323:25–39
Pakdaman K, Thieullen M, Wainrib G (2010) Fluid limit theorems for stochastic hybrid systems with application to neuron models. Adv Appl Probab 42(3):761–794
Paulus W, Baur I, Beutler AS, Reeves SA (1996) Diffuse brain invasion of glioma cells requires beta 1 integrins. Lab Investig J Tech Methods Pathol 75(6):819–826
Riedler MG (2011) Spatio-temporal stochastic hybrid models of biological excitable membranes. Ph.D. thesis, Heriot-Watt University
Rudnicki R, Tyran-Kamińska M (2017) Piecewise deterministic processes in biological models. Springer
Ruzicka M (2004) Fixpunktsätze. Nichtlineare Funktionalanalysis: Eine Einführung, pp 1–32
Scott M, Żychaluk K, Bearon R (2021) A mathematical framework for modelling 3d cell motility: applications to glioblastoma cell migration. Math Med Biol J IMA 38(3):333–354
Showalter RE (2013) Monotone operators in Banach space and nonlinear partial differential equations, vol 49. American Mathematical Society
Sidani M, Wessels D, Mouneimne G, Ghosh M, Goswami S, Sarmiento C, Wang W, Kuhl S, El-Sibai M, Backer JM et al (2007) Cofilin determines the migration behavior and turning frequency of metastatic cancer cells. J Cell Biol 179(4):777–791. https://doi.org/10.1083/jcb.200707009
Stroock DW (1974) Some stochastic processes which arise from a model of the motion of a bacterium. Z Wahrscheinlichkeitstheorie Verwandte Geb 28(4):305–315
Sun S, Titushkin I, Cho M (2006) Regulation of mesenchymal stem cell adhesion and orientation in 3d collagen scaffold by electrical stimulus. Bioelectrochemistry 69(2):133–141
Swan A, Hillen T, Bowman JC, Murtha AD (2018) A patient-specific anisotropic diffusion model for brain tumour spread. Bull Math Biol 80(5):1259–1291
Swanson KR, Alvord EC Jr, Murray J (2000) A quantitative model for differential motility of gliomas in grey and white matter. Cell Prolif 33(5):317–329
Swanson KR, Bridge C, Murray J, Alvord EC Jr (2003) Virtual and real brain tumors: using mathematical modeling to quantify glioma growth and invasion. J Neurol Sci 216(1):1–10
Tamai S, Ichinose T, Tsutsui T, Tanaka S, Garaeva F, Sabit H, Nakada M (2022) Tumor microenvironment in glioma invasion. Brain Sci 12(4):505
Tonn J, Wunderlich S, Kerkau S, Klein C, Roosen K (1998) Invasive behaviour of human gliomas is mediated by interindividually different integrin patterns. Anticancer Res 18(4A):2599–2605
Tracqui P (1995) From passive diffusion to active cellular migration in mathematical models of tumour invasion. Acta Biotheor 43(4):443–464
Tracqui P, Cruywagen G, Woodward D, Bartoo G, Murray J, Alvord E Jr (1995) A mathematical model of glioma growth: the effect of chemotherapy on spatio-temporal growth. Cell Prolif 28(1):17–31
Uatay A (2019) Multiscale mathematical modeling of cell migration: from single cells to populations. Ph.D. thesis, Technische Universität Kaiserslautern
Wang Z, Butner JD, Kerketta R, Cristini V, Deisboeck TS (2015) In: Seminars in cancer biology, vol 30, Elsevier, pp 70–78
Wesseling P, Capper D (2018) Who 2016 classification of gliomas. Neuropathol Appl Neurobiol 44(2):139–150

Yagi A (2009) Abstract parabolic evolution equations and their applications. Springer